D MESON DECAY STUDIES AT THE Ψ''

David Hitlin

California Institute of Technology

Pasadena, California 91125

representing

The Mark III Collaboration*

The status of our understanding of the weak decay mechanism for charmed mesons is discussed in the light of new, preliminary results from the Mark III at SPEAR, taken at the Ψ'' resonance. Branching ratios for several previously unobserved Cabibbo-allowed and suppressed decay modes of D^+ and D° are presented. A new analysis of the Dalitz plots of decays to pseudoscalar vector channels is discussed. An analysis of the electron content of tracks recoiling against reconstructed hadronic D decays yields new measurements of D^+ and D° semileptonic branching fractions and of the ratio of D^+ and D° lifetimes.

1. INTRODUCTION

The last few years have seen a great deal of effort on both theoretical and experimental aspects of the weak decays of heavy quarks. This effort was stimulated, in large part, by work from Mark II[1] and DELCO[2] at SLAC, which showed that the lifetimes of the charged and neutral D mesons were not equal, as had been expected in the most widely discussed picture, the light quark spectator model. The Mark II also provided other surprises in hadronic D decays. The ratio of $D^\circ \to \overline{K}^\circ\pi^\circ$ and $D^\circ \to K^-\pi^+$ branching fractions, expected to be less than a percent, was found to be 0.75 ± 0.35, and the two

Cabibbo-suppressed modes[3] $D^* \to K^-K^+$ and $D^* \to \pi^-\pi^+$, expected to occur with approximately equal branching ratios, were found to proceed in the ratio 3.4. These unexpected results led to a long series of measurements at other laboratories which have indeed established that D^* and D^+ lifetimes are not equal. These experiments, using emulsions, bubble chambers, silicon strip devices and high precision vertex chambers, have now accumulated a few hundred total examples of D decays. A compilation of these results[4] is shown in Figures 1 and 2. While uncertainties in individual measurements are large, agreement is, in the main, satisfactory, yielding world averages of

$$\tau(D^*) = 3.7^{+0.5}_{-0.4} \times 10^{-13} \text{ sec},$$

and

$$\tau(D^+) = 8.9^{+1.4}_{-1.0} \times 10^{-13} \text{ sec}$$

for individual lifetimes. The world average ratio, excluding the new Mark III measurement to be discussed below, is thus

$$\tau(D^+)/\tau(D^*) = 2.5 \pm 0.6 .$$

D meson lifetimes are indeed not equal.

Measurement of the lifetime of the charm-strange F^+ meson lifetime has had as checkered a history as has measurement of the F^+ meson mass. At this point, the only reliable measurement seems to be the 3 events from the ACCMOR collaboration which yield

$$\tau(F^+) = 3.2^{+3.0}_{-1.3} \times 10^{-13} \text{ sec}.$$

Thus, with large uncertainty, the F^+ lifetime appears to be more similar to the D^* lifetime than to the D^+ lifetime.

The new, more precise Mark III measurements of the D^+ and D^* semileptonic branching ratios confirm the D lifetime difference, and further allow us to understand whether the difference is due to an increase in the D^* decay width or an inhibition of the D^+ width. The

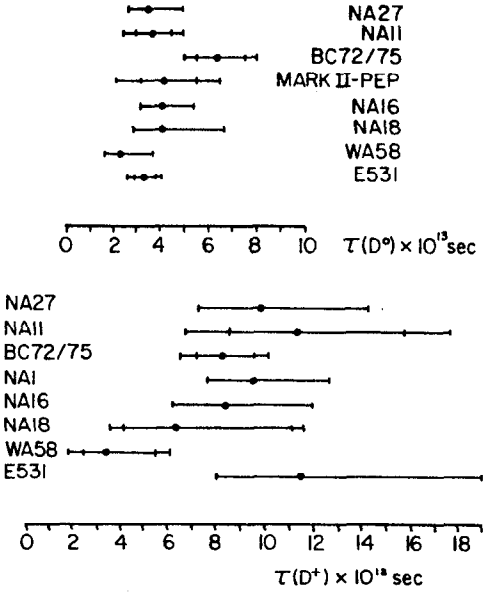

Fig. 1 Compilation of experimental results on D^* and D^+ lifetimes
a) D^* lifetime measurements and
b) D^+ lifetime measurements.

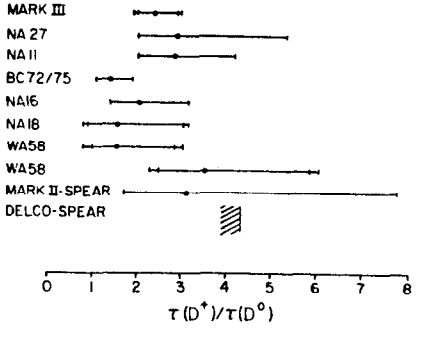

Fig. 2 Ratio of $\tau(D^+)/\tau(D^*)$. Note that Mark II-SPEAR, DELCO-SPEAR and Mark III measurements are ratios of semileptonic branching fractions.

precision is such that the current measurement of the lifetime ratio is, by itself, an improvement on the precision of the previous world average. The new Mark III data also play an important role in increasing our experimental understanding of exclusive hadronic decays of the D mesons. Such an understanding is needed to choose among the several explanations advanced for the non-equality of the D meson lifetimes.

Samples of D mesons produced in pairs at the Ψ'' resonances provide several advantages for the study of weak decay processes. The first is that since the Ψ'' resonance decays completely into $D\bar{D}$ pairs, a measurement of the Ψ'' cross section in principle allows the direct extraction of branching ratios, as opposed to the $\sigma \times BR$ measurements done in hadron- or photo-production. In practice, however, normalization using this technique has proved difficult. The fact that the D mesons are produced in pairs also allows the measurement of absolute branching ratios. The technique is straightforward: Having reconstructed a D^* or $D^\pm$ via a hadronic decay mode (the tag), counting the fraction of recoil decays into a particular channel gives an absolute measurement of that branching fraction, independent of the production cross section. This technique was exploited by the Mark II in measuring the D semileptonic branching ratios, but the detection efficiency and sample size were insufficient to allow application of this approach to hadronic branching fractions. The Mark III has been able to make measurements of absolute branching fractions for two D hadronic decay modes in this way.

The improved precision of hadronic branching fractions determinations, together with the new Cabibbo-allowed and -suppressed modes seen by the Mark III makes it possible to deepen our understanding of the contributions of various decay attributes. By taking particular ratios of branching fractions, it is possible to isolate the color suppression mechanism, QCD corrections to operator coefficients, SU(3) breaking terms and the isospin content of the final state. New light is also shed on the mechanism of Cabibbo-suppressed decay by the observation of four new suppressed D^+ hadronic decay modes.

2. THE MARK III DETECTOR

A major motivation for construction of the Mark III detector at SPEAR was the desire to gather a sufficiently large sample of D decays to lead us to a deeper understanding of the mechanism of charmed particle decays by the technique described above. It is this sample which will be discussed in this report. These studies require complete reconstruction of hadronic final states; the Mark III was therefore designed to cover a large solid angle with good tracking, good photon detection efficiency and the best possible particle identification. The magnetic field is a .4T solenoid. Charged particle tracking is provided by a small low mass drift chamber of four layers which also serves as a trigger chamber, and a large cylindrical drift chamber with 30 layers. The first twelve of these provide dE/dx information for particle identification. The following six layers are arranged in groups of three planes; four layers are axial, two provide z position measurements by small angle stereo. Charge division measurements on the trigger chamber and 3 additional layers provide additional z information. The tracking system covers 85% of 4π with a momentum resolution of $\sigma(p)/p = 1.5\% \sqrt{1+p^2(\mathrm{GeV}^2)}$. Further particle identification is provided by 48 scintillation counters, covering 80% of 4π, which have a time resolution of 180 psec. Photon detection, covering 95% of 4π, is provided by a proportional chamber readout shower counter placed inside the solenoid. This consists of 24 layers of 0.5 radiation length lead, read out in 12 depth samples. The energy resolution is $\sigma(E)/E = 18\%/\sqrt{E(\mathrm{GeV})}$. Most importantly for exclusive state reconstruction, the photon reconstruction efficiency is greater than 75% at 75 MeV and reaches 100% at 100 MeV. Muon identification is provided by two layers of proportional tubes which cover 65% of 4π. Further details on the Mark III detector may be found elsewhere.[5]

The Ψ'' sample reported on here consists of 8.1 pb^{-1} for the hadronic decay studies and 8.6 pb^{-1} for the semileptonic branching ratio studies. This is $\sim$3 times the Mark II sample. Improved reconstruction efficiency has, however, resulted in a much larger increase

in the number of D tags.

3. MODELS FOR D MESON DECAY

3.1 Inclusive Decays

Cabibbo-allowed semileptonic decays of D decays occur through β decay of the charmed quark as shown in Figure 3a, unambiguously characterized in first order by a decay width

$$\Gamma(c \to l\bar{\nu}_l X) = \frac{G_F^2 m_c^5}{192\pi^3} .$$

Cabibbo-suppressed semileptonic decays may also occur via this mechanism (Fig. 3b) or, in the case of the D^+ only, via an annihilation diagram (Fig. 3c). Purely leptonic decays are helicity-suppressed, and will not be discussed further here.

To the extent that Cabibbo-suppressed decays may be neglected, the ratio of D^* and D^+ semileptonic branching ratios may be interpreted as the ratio of lifetimes [6]:

$$\frac{B(D^+ \to e^+X)}{B(D^* \to e^+X)} = \frac{\Gamma(D^+ \to e^+X)/\Gamma_{tot}(D^+)}{\Gamma(D^* \to e^+X)/\Gamma_{tot}(D^*)} = \frac{\Gamma_{tot}(D^*)}{\Gamma_{tot}(D^+)} = \frac{\tau(D^+)}{\tau(D^*)} ,$$

as both D^+ and D^* Cabibbo-allowed semileptonic decays proceed via a spectator process in which the same $c \to s$ transition is involved.

Cabibbo-allowed hadronic decays occur via an interaction described by the following effective non-leptonic Hamiltonian [7]:

$$H_{NL}^{eff} = \frac{G_F}{\sqrt{2}} V_{cs}^* V_{ud} (c_+ O_+ + c_- O_-) ,$$

where

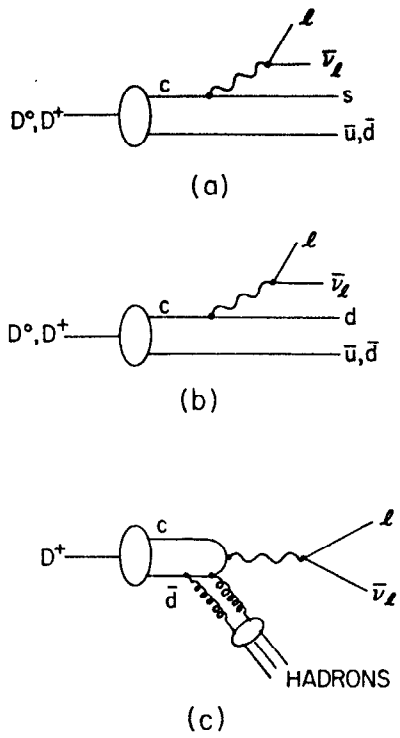

Fig. 3 Quark diagrams representing inclusive semileptonic decays of D mesons:
a) Cabibbo-allowed spectator diagram,
b) Cabibbo-suppressed spectator diagram, and
c) Cabibbo-suppressed annihilation diagram (D^+ only).

$$O_\pm = \tfrac{1}{2}[(\bar{u}d)_L(\bar{s}c)_L \pm (\bar{s}d)_L(\bar{u}c)_L] .$$

The notation $(\bar{q}_1 q_2)_L$ represents the appropriate V-A interaction for each $\bar{q}_1 q_2$ pair. The Hamiltonian can be rewritten as

$$H_{NL}^{eff} = \frac{G_F}{\sqrt{2}} V_{cs}^* V_{ud} \left\{ \frac{c_+ + c_-}{2} (\bar{u}d)_L(\bar{s}c)_L + \frac{c_+ - c_-}{2} (\bar{s}d)_L(\bar{u}c)_L \right\} .$$

In the absence of strong interactions, the coefficients c_+ and c_- are equal: $c_+ = c_- = 1$, so that only the first term in the effective Hamiltonian survives. This is the light quark spectator model, which leads to equal lifetimes for the D mesons, as well as to a 20% semileptonic branching fraction. Strong interaction effects are expected to increase c_- with respect to c_+. Since the terms in H_{NL}^{eff} which multiply c_- transform as a $\underline{6}$ of SU(3), which is contained in the $\underline{\underline{20}}$ representation of SU(4), while the c_+ operators transform as a $\underline{\underline{15}}$, which is contained in the $\underline{\underline{84}}$ of SU(4), the increase in c_- over c_+ has come to be called $\underline{6}$ *dominance*.[8] This is analogous to octet dominance in K meson decay, which is thought to be the origin of the $\Delta I = \frac{1}{2}$ rule.

The calculation of strong interaction modifications to the couplings and their effect on inclusive and exclusive decays, suffers from technical limitations. QCD allows hard gluon corrections to be estimated, but soft corrections, which as we shall see may play a role, are less tractable.

The one loop hard gluon corrections may be summed using renormalization group techniques.[9] In leading log approximation the result is

$$c_\pm = \left[\alpha_s(\mu^2)/\alpha_s(m_W^2)\right]^{d_\pm}$$

where the anomalous dimensions $d_- = -2d_+ = \frac{12}{33 - 2N_f}$, depend on the number of quark flavors N_f, which will henceforth be taken as 6. Note that $c_- c_+^2 = 1$. The exact renormalization point, μ^2, is somewhat uncertain for charm decay, as is the appropriate value of Λ_{QCD}, which enters through the definition of α_s (in one-loop approximation):

$$\alpha_s(Q^2) = \frac{4\pi}{\left(11 - \frac{2N_f}{3}\right) \ln\left(\frac{Q^2}{\Lambda_{QCD}^2}\right)} .$$

The dependence of the ratio c_-/c_+ on μ and Λ_{QCD} (in the $\overline{MS}$ scheme) is shown in Fig. 4, in leading log (LL) approximation. For $\mu = 1.5$ GeV and $\Lambda_{QCD} = 250$ MeV, we expect $c_-/c_+ = 2.72$. The cancellation of the second term in H_{NL}^{eff} thus no longer obtains. It is convenient to use a Fierz transformation and the octet algebra of the gluons to rewrite one of the four-quark operators:

$$(\bar{u}\lambda^a d)_L(\bar{s}\lambda^a c)_L = 2(\bar{u}c)_L(\bar{s}d)_L - \frac{2}{3}(\bar{u}d)_L(\bar{s}c)_L .$$

The renormalization of c_- and c_+ thus explicitly leads to a non-leptonic enhancement, since

$$\Gamma(c \to s u \bar{d}) = (2c_+^2 + c_-^2)\Gamma(c \to s l \bar{\nu}) ,$$

or

$$B(c \to eX) = \frac{1}{2 + 2c_+^2 + c_-^2} .$$

For these values of μ and Λ_{QCD}, $B(c \to eX)$ is reduced from the naive value of 20% to 16%. The lifetimes of D^0, D^+ and F^+ mesons remain, in this picture, identical.

This picture is far too simple, for several reasons. Even granting the neglect of non-perturbative effects for the moment, several non-negligible corrections have not been incorporated. The first of these is the next-to-leading log (NLL) terms, which have been calculated.[10] The results of this complex calculation can be summarized as

$$c_\pm(NLL) = c_\pm(LL)\left[1 + \frac{\alpha_s(\mu^2) - \alpha_s(M_W^2)}{\pi}\rho_\pm\right] ,$$

where $\rho_\pm$ depend on the number of quark flavors. For $N_f = 6$, $\rho_+ = -0.574$, $\rho_- = 1.65$. In the charm regime, these corrections are rather important. Figure 5 shows the ratio of c_- to c_+ with the NLL corrections included. At low μ, there are substantial modifications, with a rapid dependence on the (uncertain) value of Λ_{QCD}. At $\mu = 1.5$ GeV and $\Lambda_{QCD} = 250$ MeV, we now have $c_-/c_+ = 3.45$, giving a semileptonic branching ratio of $B(c \to eX) = 12\%$.

Radiative corrections have yet to be incorporated. These corrections, due to real and virtual gluon emission, are different for hadronic and semileptonic decays and thus further modify the semileptonic branching ratio. These calculations have also been done.[11] The two-loop, radiatively-corrected non-leptonic enhancement factor is then

$$\frac{2c_+^2 + c_-^2}{3}\left[1 + \frac{2}{3}\frac{\alpha_s(\mu^2)}{\pi}h\right] , \text{ with}$$

$$h = -\left[\pi^2 - \frac{31}{4}\right] + \frac{19}{4}\frac{c_-^2 - c_+^2}{2c_+^2 + c_-^2} + 3\frac{\alpha_s(\mu^2) - \alpha_s(M_W^2)}{\alpha_s(\mu^2)}\frac{2c_+^2\rho_+ + c_-^2\rho_-}{2c_+^2 + c_-^2} .$$

These corrections lower $B(c \to eX)$ to $\sim 11\%$.

The last correction to be considered involves the fact that quark masses have, to this point, been neglected. These corrections are sensitive to the values of quark masses used, through the sensitivity of the decay widths to the available phase space. They tend to increase the expected semileptonic branching ratio, since the hadronic width is affected more than the semileptonic width. These corrections, which can also be the source of slightly different semielectronic and semimuonic branching ratios, are not negligible. They tend to raise the expected value of $B(c \to eX)$ up to the range of 13-16%. Note once again, however, that none of these effects has produced a difference between the expected D^* and D^+

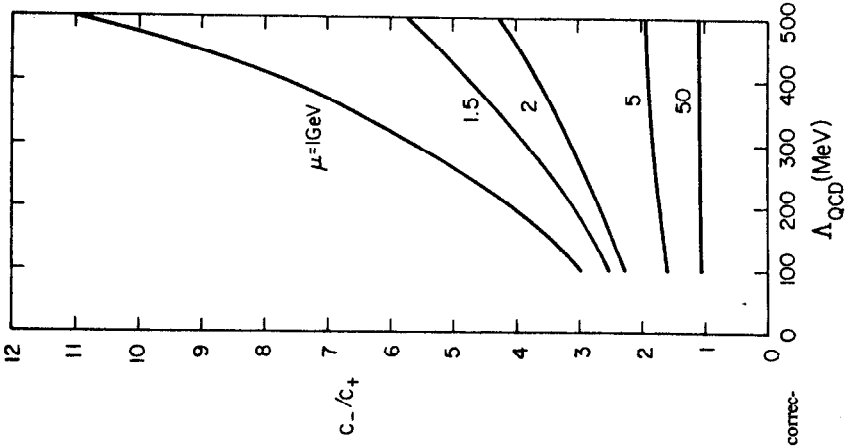

Fig. 4 Ratio of the operator coefficients c_- and c_+ in leading log approximation as a function of Λ_{QCD} for various values of the mass scale μ.

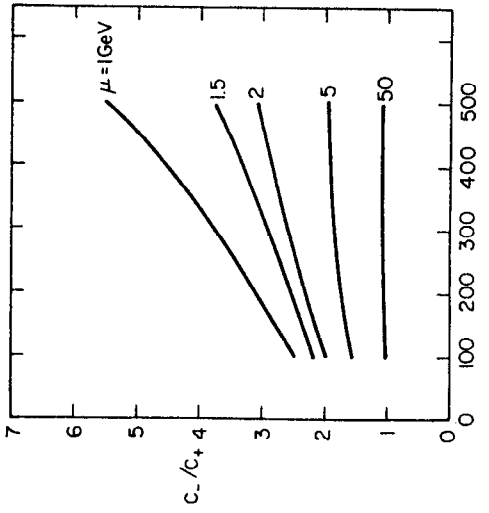

Fig. 5 Ratio of the operator coefficients c_- and c_+ including next-to-leading log corrections, as a function of Λ_{QCD} for various values of μ.

semileptonic branching ratios or lifetimes.

It is worth remembering that the hard gluon estimates of the renormalization of c_+ and c_- still neglect non-perturbative effects.[12] We will see later that there is indeed some experimental evidence that c_- and c_+ in fact differ from these estimates, even with all the effects enumerated above included.

In order to produce differing charmed meson lifetimes, we must invoke additional effects. These are of two kinds, one pertinent to the D^+ and one to the D^*. As the spectator quark which accompanies the initial c quark differs in the two mesons, the final state after the weak transition is also distinct. Figure 6 shows the quark content of the final state in D^* and D^+ hadronic decay resulting from the two terms in H_{NL}^{eff}. Note that for the D^*, the two amplitudes are distinct, while in the D^+ case, they are identical. This brings up the interesting possibility that the two D^+ amplitudes can interfere destructively,[13] thus lengthening the D^+ lifetime

$$\Gamma(D^+) = \Gamma_{SL} + \Gamma_{NL} + \Gamma_{int} \ ,$$

and increasing the D^+ semileptonic branching ratio. This so-called "Pauli interference" depends on the overlap of the quark wave functions:

$$\Gamma_{int} = -(c_-^2 - 2c_+^2)\frac{G_F^2}{\pi} M_B^2 \ |\Psi(0)|^2 \ .$$

The wave function at the origin can be evaluated in bag models or using QCD sum rules. It is, of course, related to the D meson decay constant, f_D. In the model cited above:

$$f_B^2 = 12 \frac{|\Psi(0)|^2}{M_D} \ .$$

With plausible values of f_D = (200–300) MeV, and the renormalized c_+ and c_- coefficients, substantial changes in the D^+ semileptonic branching ratio can occur:

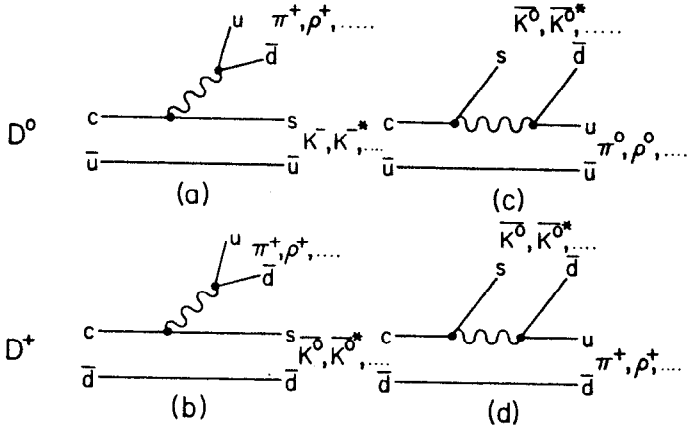

Fig. 6 Quark diagrams representing the hadronic decays of D^* and D^+ mesons in the light quark spectator model.

a),b) Amplitudes proportional to $c_- + c_+$.

c),d) Amplitudes proportional to $c_- - c_+$.

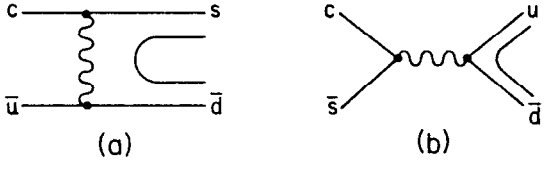

Fig. 7 Additional amplitudes for D decays, which are suppressed by helicity conservation in the absence of gluon contributions:

a) W exchange diagram for D^* decay and

b) Annihilation diagram for F^+ decay.

$$B(D^+ \to eX) = \frac{1}{2 + 2(1+\alpha)c_+^2 + (1-\alpha)c_-^2}$$

where

$$\alpha \equiv \frac{\Gamma_{int}}{\Gamma_{NL}} \cdot \frac{2c_+^2 + c_-^2}{2c_+^2 - c_-^2} \ .$$

Thus, the Pauli interference effect increases $B(D^+ \to e^+X)$ and lengthens the D^+ lifetime. We will defer comparison of these ideas with data until after detailed discussion of the new Mark III results.

The other possibility is that the D^* decay rate is enhanced,[14] since there is an amplitude for D^* decay which is forbidden to the D^+. This is the so-called W exchange diagram shown in Fig. 7a, which in lowest order should be small due to helicity suppression at the light quark vertex. There is also a related W annihilation diagram for F^+ decay, shown in Fig. 7b.

The contribution of the exchange diagram to the D^* width is then given by Γ_A:

$$\Gamma(D^*) = \Gamma_{SL} + \Gamma_{NL} + \Gamma_A \ .$$

As Γ_A is strictly positive, the D^* decay rate is enhanced and its semileptonic branching ratio is decreased by the W exchange diagram.

Two distinct mechanisms have been advanced for the lifting of helicity suppression. The first is the explicit radiation of soft gluons,[15] which produces a contribution to the D^* width given by

$$\frac{\Gamma_A}{\Gamma_{NL}} \simeq \frac{2\pi\alpha_s}{27} \frac{(c_+ + c_-)}{(2c_+^2 + c_-^2)} \left[\frac{f_D}{m_u}\right]^2 \sim 0.03\text{–}0.09 \ .$$

A rather larger effect is estimated in the second picture, which ascribes the removal of the suppression to a large intrinsic octet gluon component in the D^* wavefunction[16]:

$$\frac{\Gamma_A}{\Gamma_{NL}} \simeq \frac{4\pi^2}{3} \frac{(c_+ + c_-)^2}{(2c_+^2 + c_-^2)} \left[\frac{f_D}{M_D}\right]^2 \sim 0.2\text{–}0.6 \ .$$

A still larger ratio ($\sim$1.5) has been estimated using a QCD multipole expansion formalism.[17]

Again, we will defer detailed comparison of these approaches until after discussion of the experimental data. It is important to point out, however, that the measurement of semileptonic branching ratios as well as the D lifetimes is important in deciding whether the lack of equality of lifetimes is due to enhancement of the D^* width or suppression of the D^+ width, or a combination of both.

In summary, we have identified three possible contributions to non-equal D^* and D^+ lifetimes:

1) Pauli interference in D^+ decay,

2) Removal of helicity suppression of W exchange amplitudes in D^* decay and

3) 6 dominance ($c_- >> c_+$) due to renormalization of the operator coefficients and non-perturbative effects.

Both 2) and 3) can result from pre-asymptotic, non-perturbative effects, which are difficult to calculate, but whose existence can be established phenomenologically.

3.2 Exclusive Decays

Exclusive decays provide further information on the decay mechanism. The surprisingly large decay rate for $D^* \to \overline{K}^*\pi^*$ shows that color suppression (the dominance of amplitude a over b in Fig. 5) is not as effective as a naive estimate would indicate. The presence of color-octet gluons in the meson wave function, or the explicit radiation of gluons by the light quark, could also be responsible for color suppression not being as stringent as expected. This dilution of the suppression can occur either through communication of color

over short distances within the meson wave function or through enhancement of non-spectator processes by removal of helicity suppression. A search for other decays which occur mainly through W exchange amplitudes, such as $D^+ \to \overline{K}^{*0}\varphi^+$ or $\overline{K}^{*0}K^+$ can shed light on this question.[18]

Hadronic final states formed through spectator diagrams may be either $I = \frac{1}{2}$ or $I = \frac{3}{2}$, while those produced by W exchange diagrams are purely $I = \frac{1}{2}$. The study of ratios of particular exclusive channels related by isospin can be used to isolate the $I = \frac{3}{2}$ and $\frac{1}{2}$ contributions.

The valence quarks produced in $D \to K\pi$, $D \to K\rho$ and $D \to K^*\pi$ decays are identical. As the $K\pi$ states are $L = 0$ while the $K\rho$ and $K^*\pi$ are $L = 1$, different matrix elements will govern each group. However, within the groups, ratios of branching fractions can shed light on the decay process. Three combinations of final state particles are possible in each group:

$$(-+) \equiv D^+ \to K^-\pi^+,\ K^{*-}\pi^+,\ K^-\rho^+,$$

$$(00) \equiv D^+ \to \overline{K}^0\pi^0,\ \overline{K}^{*0}\pi^0,\ \overline{K}^0\rho^0 \text{ and}$$

$$(0+) \equiv D^+ \to \overline{K}^0\pi^+,\ \overline{K}^{*0}\pi^+,\ \overline{K}^0\rho^+ .$$

Since the weak Hamiltonian changes isospin by one unit, the D meson decay amplitudes within each group must obey a triangle relation:

$$A(-+) + \sqrt{2}A(00) = A(0+) .$$

Each amplitude is a combination of complex $I = \frac{1}{2}$ and $I = \frac{3}{2}$ amplitudes[19]:

$$A(00) = \sqrt{\frac{1}{3}}\,A_{1/2}e^{i\delta_{1/2}} + \sqrt{\frac{2}{3}}\,A_{3/2}e^{i\delta_{3/2}},$$

$$A(-+) = -\sqrt{\frac{2}{3}}\,A_{1/2}e^{i\delta_{1/2}} + \sqrt{\frac{1}{3}}\,A_{3/2}e^{i\delta_{3/2}} \quad \text{and}$$

$$A(0+) = \sqrt{3}\,A_{3/2}e^{i\delta_{3/2}} .$$

In the absence of final state interactions, the $A_{1/2}$ and $A_{3/2}$ amplitudes are relatively real.

If we neglect final state interactions for the moment, these amplitudes can be written in terms of the contribution of spectator diagrams (with coefficients c_-, c_+) and the W exchange diagram (coefficient g):

$$A(00) = \frac{1}{3\sqrt{2}}\,(2c_+ - c_- - g)\,A,$$

$$A(-+) = \frac{1}{3}\,(2c_+ + c_- + g)\,A \quad \text{and}$$

$$A(0+) = \frac{4}{3}\,c_+ A .$$

A distinct overall amplitude, $A(PP)$ or $A(P_iV_j)$, of course applies for each of the three ($K\pi$, $K^*\pi$, $K\rho$) groups. Note that the W exchange amplitude, g, contributes only to an $I = \frac{1}{2}$ final state.

Analysis of the ratios

$$\frac{\Gamma(D^+ \to \overline{K}^0\pi^+)}{\Gamma(D^+ \to K^-\pi^+)} = \frac{\Gamma(D^+ \to \overline{K}^{*0}\pi^+)}{\Gamma(D^+ \to K^{*-}\pi^+)} = \frac{\Gamma(D^+ \to \overline{K}^0\rho^+)}{\Gamma(D^+ \to K^-\rho^+)}$$

$$= \tfrac{1}{2}\left[\frac{2c_+ - c_- - g}{2c_+ + c_- + g}\right]^2$$

and

$$\frac{\Gamma(D^+ \to K^-\pi^+)}{\Gamma(D^+ \to \overline{K}^0\pi^+)} = \frac{\Gamma(D^+ \to K^{*-}\pi^+)}{\Gamma(D^+ \to \overline{K}^{*0}\pi^+)} = \frac{\Gamma(D^+ \to K^-\rho^+)}{\Gamma(D^+ \to \overline{K}^0\rho^+)}$$

$$= \left[\frac{2c_+ + c_- + g}{4c_+}\right]^2$$

can then serve to isolate particular coefficients.

Note that in the unlikely limit of a pure W exchange process, which produces an $I = \frac{1}{2}$ final state, these ratios are $\frac{1}{2}$ and ∞, respectively. In a more conventional picture in which spectator diagrams alone contribute, the first group of ratios is sensitive to color suppression through the difference of c_+ and c_-. It is of course possible that the observed lack of color suppression in these decays can result both from the values of c_+ and c_- and from the W exchange amplitude which is not expected to exhibit this effect.

4. EXPERIMENTAL RESULTS

4.1 Cabibbo-allowed Non-leptonic Decays

Reconstruction of a large sample of D non-leptonic decays has been a major goal of the Mark III effort at the Ψ''. This sample is needed for the recoil studies of absolute hadronic and semileptonic branching ratios which are described below, but the improvement of the precision of hadronic branching fractions and the search for new decay modes is interesting in its own right. Comparison of rates for related decay modes can help to shed light on the decay mechanism since, for example, spectator diagrams produce $I = \frac{1}{2}$ and $I = \frac{3}{2}$ $K\pi$ final states while exchange diagrams produce only $I = \frac{1}{2}$ states.

The existence of the Ψ'', which decays into $D\bar{D}$ pairs close to threshold, allows reconstruction of D hadronic decays with mass resolution of a few MeV. The technique is to first identify tracks originating close to the primary event vertex as K's or π's by measurement of time-of-flight (π assumed otherwise) and then to calculate the invariant mass for appropriate GIM and Cabibbo-allowed combinations. A loose cut on the D mass is next made, and the so-called "beam-constrained mass"

$$M_{BC} = \sqrt{E_{beam}^2 - P_D^2} \ ,$$

is computed. The resolution in M_{BC} ($\sim$3 MeV) is substantially better than that in invariant mass ($\sim$12 MeV), as the uncertainty in the storage ring beam energy is much smaller than that for the reconstructed E_D. This technique is applied to each of the charged particle decay modes. Decays containing K_s^0 are reconstructed through the $K_s^0 \to \pi^+\pi^-$ channel. For modes involving a π^0, a 2C fit is performed: the total energy of charged particles and photons is constrained to E_{beam}, while the photons are constrained to the π^0 mass. A similar approach is used for decays involving η's, which will not be discussed here.

Figure 8 shows the beam-constrained mass distributions for five Cabibbo-allowed D^0 and five D^+ decays. Figure 9 shows the beam-constrained mass for the rare, although allowed, mode $D^0 \to \bar{K}^0\pi^0$.

Table I shows the Mark III values of $\sigma \cdot B$ for these seven D^0 and five D^+ modes, together with comparisons with previous measurements. In the case of certain small modes such as $\bar{K}^0\pi^0$ and $\bar{K}^0K^+K^-$, branching fraction results will be quoted in the text as ratios to larger related modes. This approach is more precise, and it is the ratios which are of interest for interpretation in any case. Three modes, $D^0 \to \bar{K}^0\pi^+\pi^-\pi^0$, $D^0 \to \bar{K}^0K^+K^-$ and $D^+ \to K^-\pi^+\pi^+\pi^0$ have not previously been seen, while the important mode $D^0 \to \bar{K}^0\pi^0$ had been seen previously with only a few events. Where previous measurements exist, the agreement of $\sigma \cdot B$ values is generally quite good, especially between Mark II and Mark III. The increased integrated luminosity, and improved solid angle and π^0 efficiency of the Mark III results in substantial improvements in the number of reconstructed events and the precision of $\sigma \cdot B$ measurements, especially in decay modes involving π^0's. The branching ratio values are extracted using an average of Mark II[20] and Crystal Ball[21] parameters for the Ψ'' resonance. A more detailed discussion of the extraction of D branching fractions will be

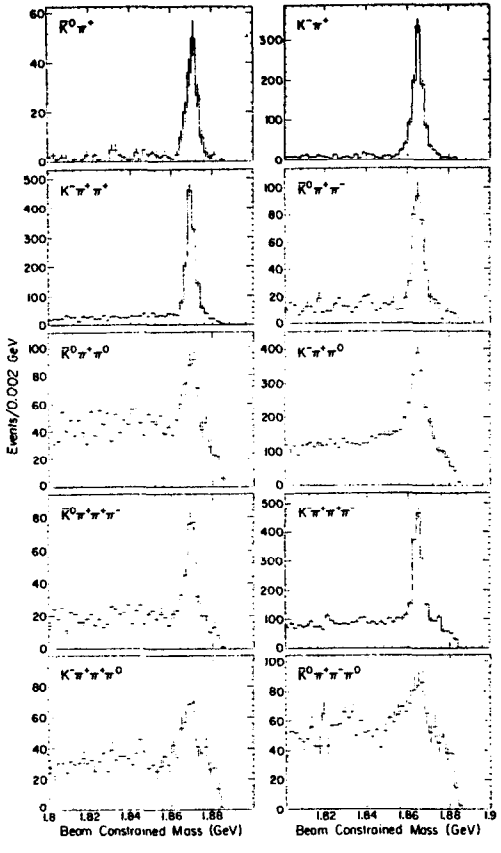

Fig. 8 Beam constrained mass distributions for five D^+ and five D^* hadronic decays.

TABLE I

Cabibbo-Allowed D Branching Ratios

Channel	Signal	ε	This Expt. $\sigma \cdot B$ (nb) $\sqrt{s}$ = 3.768 GeV	MKII[1] $\sigma \cdot B$ (nb) 3.771 GeV	LGW[22] $\sigma \cdot B$ (nb) 3.774 GeV	Br (%)*
$K^-\pi^+$	889±35	.47	.28±.01±.03	.24±.02	.25±.05	3.7±0.6±0.7
$\overline{K^*}\pi^*$	68±11		.097±.017±.015	.18±.08	—	
$\overline{K^*}K^+K^-$	12±4		.085±.028±.008	—	—	
$\overline{K^*}\pi^+\pi^-$	281±22	.09	.40±.04±.03	.30±.08	.46±.12	5.3±0.9±0.9
$K^-\pi^+\pi^*$	810±62	.21	.53±.05±.10	.68±.23	1.40±.60	7.1±1.2±1.7
$K^-\pi^+\pi^+\pi^-$	1016±44	.23	.56±.03±.06	.68±.11	.36±.10	7.5±1.2±1.4
$\overline{K^*}\pi^+\pi^-\pi^*$	126±22	.02	.76±.16±.13	—	—	10.2±2.6±2.3
$\overline{K^*}\pi^+$	142±14	.12	.15±.02±.01	.14±.03	.14±.05	2.5±0.5±0.4
$K^-\pi^+\pi^+$	1085±41	.32	.42±.02±.04	.38±.05	.36±.06	7.0±1.1±1.3
$\overline{K^*}\pi^+\pi^*$	186±23	.05	.45±.07±.07	.78±.48	—	7.6±1.6±1.8
$\overline{K^*}\pi^+\pi^+\pi^-$	187±23	.06	.38±.05±.04	.51±.18	—	6.3±1.3±1.2
$K^-\pi^+\pi^+\pi^*$	154±30	.07	.26±.06±.04	—	—	4.3±1.0±1.5

*Assumes $\sigma(D^+) = 6.0\pm0.9\pm1.0$ nb, $\sigma(D^*) = 7.5\pm1.1\pm1.2$. This is an average of the values given in Table II for Mark II[20] and Crystal Ball[21] resonance parameters.

found in the section on absolute branching ratios.

The decay $D^* \to \overline{K^*}\pi^*$ is expected to be highly color-suppressed. Indeed, with the leading log values of c_- and c_+ it is expected to occur at a rate ~1/200 that of $D^* \to K^-\pi^+$. We

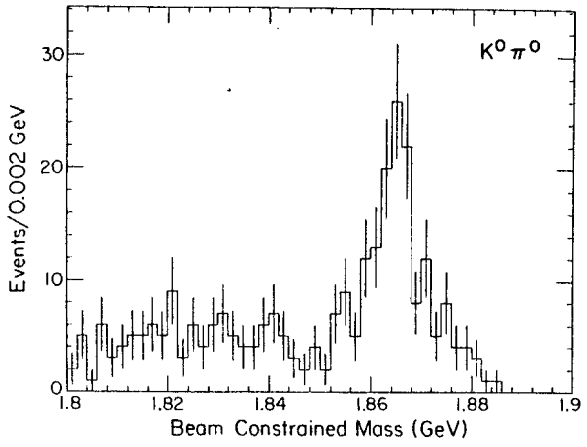

Fig. 9 Beam constrained mass distribution for the decay $D^* \to \overline{K}^*\pi^*$.

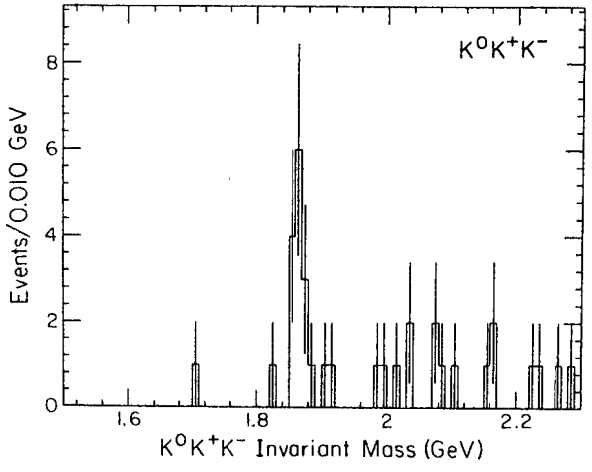

Fig. 10 Invariant mass distribution for the decay $D^* \to \overline{K}^*K^+K^-$ with $|\Delta P_D| < 50$ MeV.

find, instead,

$$\frac{B(D^* \to \overline{K}^*\pi^*)}{B(D^* \to K^-\pi^+)} = 0.35 \pm 0.07 \pm 0.07\,,$$

in rough agreement with the Mark II value of 0.75 ± 0.35, but with substantially improved precision, the measurement of $\overline{K}^*\pi^*$ being based on 68±11 events as opposed to 9±4 events. It appears that color suppression is not particularly effective in this decay.

In the valence quark approximation, in which the process of hadron formation is considered to be factorizable from the quark production process represented by H_{WL}^{μ}, the contribution of W exchange graphs to exclusive D^* channels is expected to be negligible.[23] The search for decays which occur only through W exchange is therefore particularly interesting.

If we neglect OZI violating spectator processes, the decay $D^* \to \overline{K}^*\varphi^*$ is such a channel, sometimes called a "smoking gun test."[24] The final state used is $\pi^+\pi^-K^+K$. Since the problem of π–K misidentification is particularly severe in this case, it is necessary to rely on an invariant mass reconstruction technique; the beam-constrained approach cannot be used (see also Section 4.2). The fact that the reconstructed D^* must have a unique momentum can still, however, be used to reduce background. The K_s^0 are constructed through their $\pi^+\pi^-$ decay, φ^* through K^+K^-. Figure 10 shows the invariant mass of $K_s^0K^+K^-$ with $|\Delta P_D|$, the absolute difference between the required and reconstructed D momentum, less than 50 MeV. There are 12 ± 4 events at the D^* mass. To search for $D^* \to \overline{K}^*\varphi^*$, in Fig. 11 we plot $M(K^+K^-)$ vs $M(K_s^0K^+K^-)$ within the ΔP_D cut. Figure 12 shows φ's reconstructed exclusively, demonstrating that the φ mass resolution is ~4 MeV. There are four events within $\pm 2\sigma$ of the φ mass in Fig. 11. If these events originate from $D^* \to \overline{K}^*\varphi$, we therefore find the upper limit $\sigma \cdot B(D^* \to \overline{K}^*\varphi^*) < 0.126$ nb at 95% confidence. If no $K_s^0K^+K^-$ events are $D^* \to \overline{K}^*\varphi$, the result is $\sigma \cdot B(D^* \to \overline{K}^*K^+K^-) = 0.085 \pm 0.028 \pm 0.008$ nb.

There is thus no evidence in this channel for an exclusive decay proceeding via the W exchange mechanism. The sensitivity of the search is not particularly great, however, since

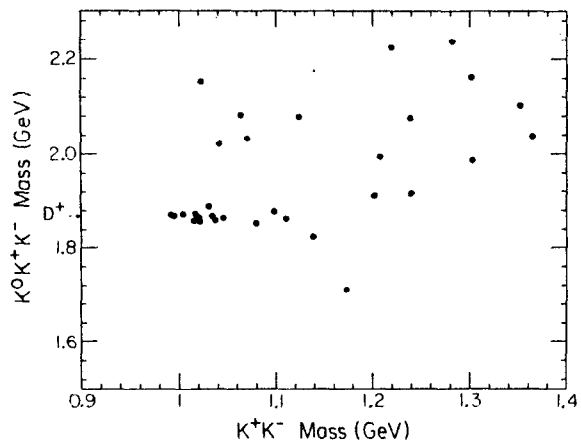

Fig. 11 Invariant mass of K^+K^- vs. mass of $\bar{K}^0K^+K^-$ with $|\Delta P_D| < 50$ MeV.

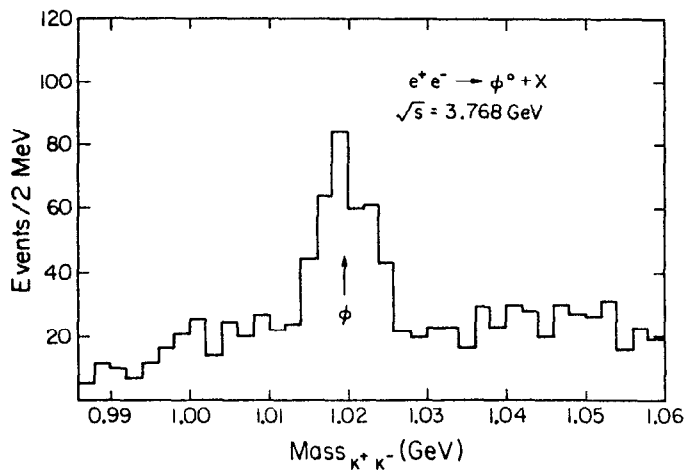

Fig. 12 The φ mesons reconstructed inclusively via the K^+K^- decay mode at the Ψ''. The mass resolution is 4 MeV.

$\bar{K}^0\varphi^0$ is heavily suppressed by phase space. Compared to the related pseudoscalar-vector decay $D^0 \rightarrow \bar{K}^0\rho$ (see Section 4.3) the limit is

$$\frac{B(D^0 \rightarrow \bar{K}^0\varphi)}{B(D^0 \rightarrow \bar{K}^0\rho)} < 1.9 \text{ at 95\% confidence level .}$$

This ratio is expected to be 0.2 - 0.5 in the W exchange model and $\sim 3 \times 10^{-4}$ in the spectator model.

4.2 Cabibbo-suppressed Decays

The non-equality of the $D^0 \rightarrow K^-K^+$ and $D^0 \rightarrow \pi^+\pi^-$ branching ratios[3] was one of the most surprising results to emerge from the Mark II. Many explanations[25] were proposed for the fact that these two modes did not, when corrected for phase space differences, occur at equal rates. Within the spectator picture, the Kobayashi-Maskawa six quark scheme allows, in principle, for differences in the effective coupling constant to $\pi^+\pi^-$ and K^+K^-. With the now well-established long b quark lifetime,[26] however, communication between the light quark and b,t sectors is known to be minimal, and explanations for the effect must be sought within the light quark sector. Annihilation diagrams contribute to Cabibbo-suppressed decays in a different pattern than they do to allowed decays. In addition, penguin diagrams,[27] possibly important in the dominance of $\Delta I = \frac{1}{2}$ amplitudes in K decay, can contribute to Cabibbo-suppressed D decays. Possible amplitudes involved in two-body allowed and suppressed D decays[28] are summarized in Figure 13.

The goal of the Mark III work in this area has been to measure the branching ratios for additional Cabibbo-suppressed hadronic modes. With a larger number of decays measured, the hope is that a pattern will emerge which sheds light on the decay mechanism.

The technique for the reconstruction of these modes is different from that employed in allowed decay modes. Since the signals are much smaller, the problem of $K^-\pi$

Fig. 13 Decay amplitudes contributing to two–body Cabibbo-allowed and Cabibbo-suppressed decays of D mesons.

misidentification assumes greater significance, and an approach which explicitly displays background due to incorrect assignment of particle type is used. The beam-constrained approach is not employed here, since, for example, a $D^* \to K^-\pi^+$ decay with the kaon called a pion would give the correct beam-constrained mass. Instead, particle assignments are made using the TOF weights, and the invariant mass is then plotted. Figure 14 shows the invariant mass plotted against the difference of the reconstructed momentum from the unique D momentum at the Ψ'', for $K^\mp K^\pm$, $K^\mp\pi^\pm$ and $\pi^\mp\pi^\pm$ modes. A cut of $|\Delta P_D| < 50$ MeV/c is then made, and the invariant mass distribution is plotted in Figure 15. While the mass resolution for this technique is a good deal worse than that for the beam-constrained approach, the advantage is that misidentified particles produce distinct peaks either above ($K^\mp K^\pm$) or below ($\pi^\mp\pi^\pm$) the D mass. The background shape can also be directly measured, using a cut on the sidebands with $60 < |\Delta P_D| < 110$ MeV/c. The background so determined is also shown in Figure 15. A maximum likelihood fit is then performed to extract the number of signal events for each mode. The mass and width of the D signal are fixed by fitting separately to the $D^* \to K^\mp\pi^\pm$ channel. The shape of the background, as determined from the procedure above, is fixed in the fit, but the magnitude is allowed to vary. The results are

$$\frac{B(D^* \to K^\pm K^\mp)}{B(D^* \to K^\mp\pi^\pm)} = 0.125 \pm 0.018 \pm 0.010$$

and

$$\frac{B(D^* \to \pi^\mp\pi^\pm)}{B(D^* \to K^\mp\pi^\pm)} = 0.038 \pm 0.010 \pm 0.005 \ .$$

Thus the non-equality of these two Cabibbo-suppressed modes is indeed confirmed, with substantially improved precision. After correcting for phase space differences, the $K^\pm K^\mp$ rate is $\sim$3.3σ above the $\tan^2\theta_c$ prediction, while the $\pi^\pm\pi^\mp$ rate is $\sim$1σ too low.

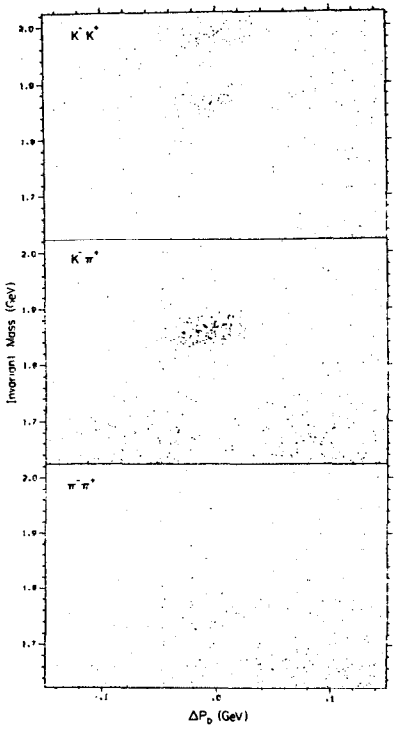

Fig. 14 Invariant mass of Cabibbo-allowed decay $D^* \to K^-\pi^+$ candidates and Cabibbo-suppressed decay candidates $D^* \to K^-K^+$, $\pi^-\pi^+$ vs ΔP_D, the difference between reconstructed and expected D^* momentum.

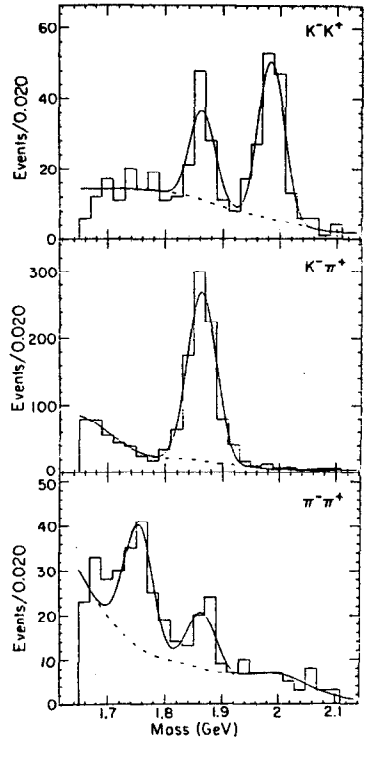

Fig. 15 Invariant mass of K^-K^+, $K^-\pi^+$ and $\pi^-\pi^+$ with $|\Delta P_D| < 50$ MeV. Note the signals at the D^* mass as well as those above and below the proper mass caused by $K^-\pi$ misidentification.

Cabibbo-suppressed hadronic decays of the $D^\pm$ are of particular interest, in that explanations of the D^*/D^+ lifetime difference which focus on cancellation of D^+ amplitudes predict that particular exclusive Cabibbo-suppressed D^+ decays would be quite large relative to their allowed partners. The invariant mass technique has therefore been used to measure the rates for the allowed decay $D^\pm \to \overline{K}^*\pi^\pm$ and the forbidden decay $D^\pm \to \overline{K}^*K^\pm$. The distribution of invariant mass vs the nominal momentum of the reconstructed $D^\pm$, shown in Fig. 16, contains clear evidence for $\overline{K}^*K^\pm$ decay of the $D^\pm$. After cutting on ΔP_D and determining background shape as was done above, the invariant mass distribution for the two decays is shown in Fig. 17. The ratio of branching ratios obtained is:

$$\frac{B(D^\pm \to \overline{K}^*K^\pm)}{B(D^\pm \to \overline{K}^*\pi^\pm)} = 0.290 \pm 0.080 \pm 0.050 \ ,$$

a surprisingly large value! This could, of course, result from an enhancement in the Cabibbo-suppressed matrix element or from an interference between the two amplitudes which contribute to the allowed decay. This will be discussed further below.

The decay $D^* \to \overline{K}^*K^*$ is particularly interesting in that it proceeds via W exchange. We observe one event consistent with this channel, and thus find the upper limit:

$$\frac{B(D^* \to \overline{K}^*K^*)}{B(D^* \to K^-\pi^+)} < 0.11 \text{ at 95\% confidence level} \ .$$

It is also possible to utilize the invariant mass approach to search for three-body Cabibbo-suppressed decays. Figure 18 shows the distribution in invariant mass vs ΔP_D for the three related decays $D^\pm \to K^\mp\pi^\pm\pi^\pm$, $D^\pm \to K^\mp K^\pm\pi^\pm$ and $D^\pm \to \pi^\mp\pi^\pm\pi^\pm$. In this case, in addition to the $|\Delta P_D| < 50$ MeV/c cut, it is necessary to exclude $\pi^+\pi^-$ masses near $M_{K_s^0}$ resulting from the allowed decay $D^\pm \to K_s^0\pi^\pm$. The projected invariant mass distributions are shown in Figure 19. Signal and background are determined by a maximum likelihood fit analogous to that described above. The ratios of branching ratios so obtained are:

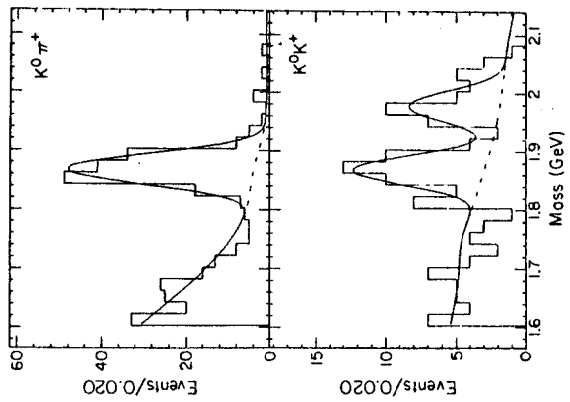

Fig. 17 Invariant mass of $\bar{K}^0\pi^+$ and $\bar{K}^0K^+$ with $|\Delta P_D| < 50$ MeV. Again, the Cabibbo-suppressed channel shows signals at the D^+ mass and a peak above this due to $K^-\pi$ misidentification.

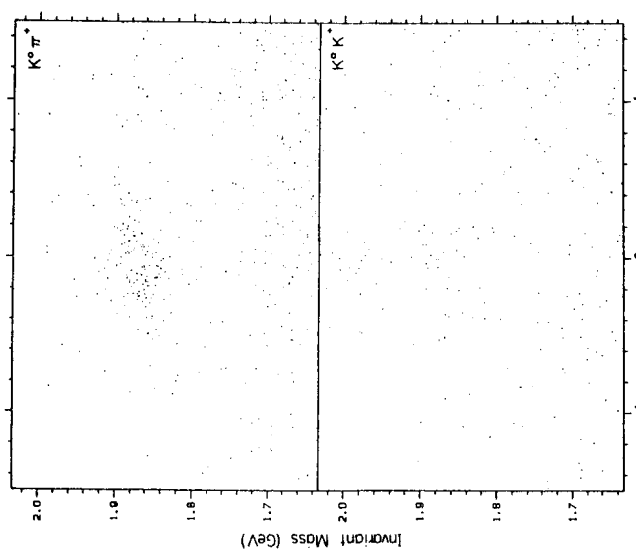

Fig. 16 Invariant mass of the Cabibbo-allowed decay candidates $D^+ \to \bar{K}^0\pi^+$ and Cabibbo-suppressed decay candidates $D^+ \to \bar{K}^0K^+$ vs ΔP_D.

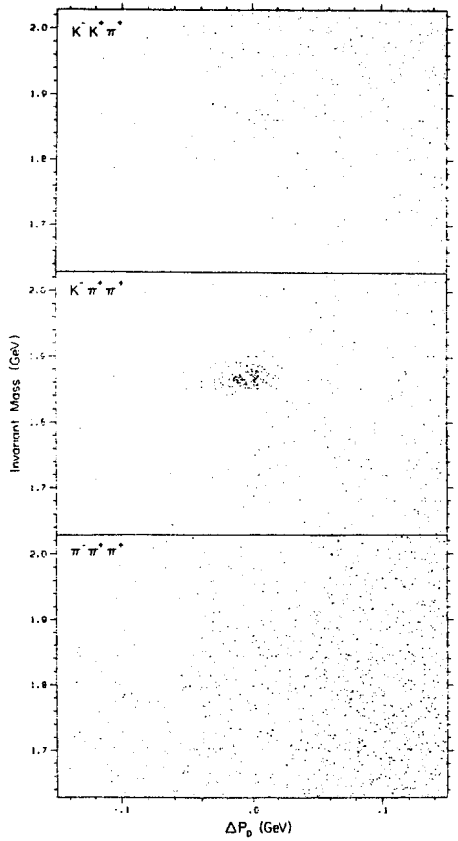

Fig. 18 Invariant mass of three body D^+ decay candidates vs ΔP_D.

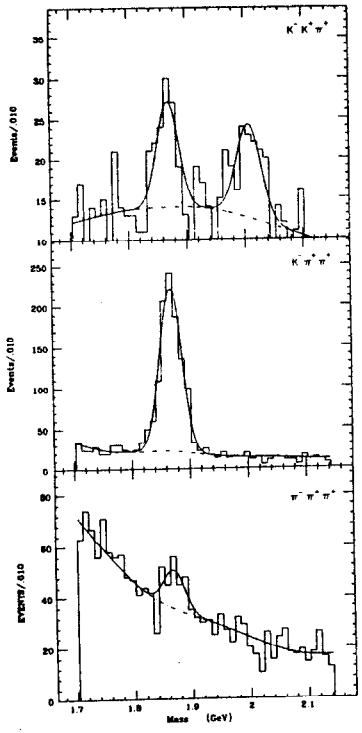

Fig. 19 Invariant mass of $K^-K^+\pi^+$, $K^-\pi^+\pi^+$ and $\pi^-\pi^+\pi^+$ with $|\Delta P_D| < 50$ MeV.

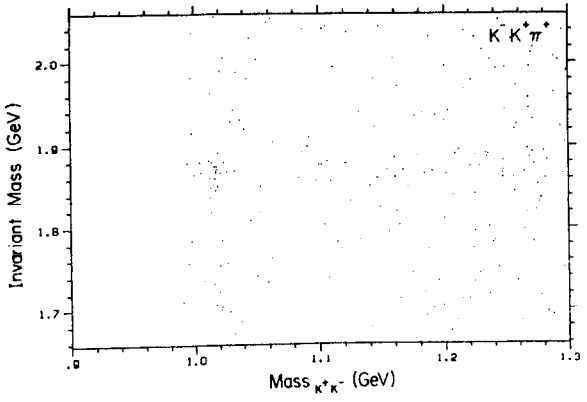

Fig. 20 Invariant mass of $K^-K^+\pi^+$ vs mass of K^-K^+. There is a clear enhancement, providing evidence for the decay $D^+ \to \varphi\pi^+$.

$$\frac{B(D^\pm \to K^\mp K^\pm \pi^\pm)}{B(D^\pm \to K^\mp \pi^\pm \pi^\pm)} = 0.072 \pm 0.024 \pm 0.015 \text{ and}$$

$$\frac{B(D^\pm \to \pi^\pm \pi^\pm \pi^\mp)}{B(D^\pm \to K^\mp \pi^\pm \pi^\pm)} = 0.059 \pm 0.016 \pm 0.010 \ ,$$

both of which are consistent with, but somewhat larger than $\tan^2\theta_c$. There are no detailed predictions for these three-body Cabibbo-suppressed decays, but nothing unusual appears to be happening in this sector.

The pseudoscalar-vector contribution to the three-body channels can also be isolated in these Cabibbo-suppressed decays. The K^+K^- mass in the $D^\pm \to K^\pm K^\mp \pi^\pm$ channel, plotted against the $K^\pm K^\mp \pi^\pm$ mass in Figure 20 shows a significant φ° signal at the D mass. With a cut requiring $M(K^+K^-) < 1036$ MeV, the $K^\pm K^\mp \pi^\pm$ channel shows a clear $D^\pm$ enhancement, leading to the result

$$\frac{B(D^\pm \to \varphi^\circ \pi^\pm)}{B(D^\pm \to K^\mp \pi^\pm \pi^\pm)} = 0.083 \pm 0.023 \pm 0.012.$$

Note that the branching ratio for the $K^\mp K^\pm \pi^\pm$ channel previously quoted has had the $\varphi^\circ \pi^\pm$ contribution subtracted. No subtraction has been made for a possible small contribution from $D^\pm \to K^{*\circ} \pi^\pm$. The suppressed $\varphi^\circ \pi^\pm$ mode shows a moderate enhancement above the naive expectation:

$$\frac{B(D^\pm \to \varphi^\circ \pi^\pm)}{B(D^\pm \to K^{*\circ} \rho^\pm)} = 0.11 \pm 0.06 \ .$$

The decay $D^\pm \to \varphi\pi^\pm$ should naively be both Cabibbo-suppressed as well as color suppressed. Thus we have here further evidence that color suppression is not operative in D decay.

4.3 Pseudoscalar-vector Decays

The quasi-two body decays $D \to K\rho$ and $D \to K^*\pi$ are governed by the same amplitude relations as are the $D \to K\pi$ channels, and thus in principle the ratios of their branch-

ing ratios provide additional information on the decay mechanism. There are six possible PV allowed channels in D decay, which may be populated in different ways from three D^+ and two D^+ three body final states. This allows an important experimental consistency check. Table II shows the pattern of $D \to PV$ decays, and previous experimental results.

The Mark II was able to extract $K\rho$ and $K^*\pi$ fractions from $D^+ \to K^-\pi^+\pi^+$ and $D^+ \to \overline{K^*}\pi^+\pi^+$ channels and the $K^-\pi^+\pi^+$ decay has also been studied by the Tagged Photon Spectrometer at FNAL. These results, both with low statistics, agreed on the $K^*\pi$ fractions, but disagreed on the $K^-\rho^+$ fraction. The Mark III has been able to study these channels with improved statistics and has been able to measure some new PV channels. While these results are still incomplete, they provide a significant new opportunity to check the isospin content of the PV decay amplitudes. Since the $I = \frac{1}{2}$ and $\frac{3}{2}$ amplitudes contribute to these decays in the same way they do to the PP amplitudes the following triangle relations must obtain:

$$A(K^{*-}\pi^+) + \sqrt{2}\, A(\overline{K^{*0}}\pi^0) - A(\overline{K^{*0}}\pi^+) = 0\,,$$

$$A(K^-\rho^+) + \sqrt{2}\, A(\overline{K^0}\rho^0) - A(\overline{K^0}\rho^+) = 0\,.$$

To extract the K^* and ρ content from the $K\pi\pi$ Dalitz plots, a maximum likelihood fit is performed. The matrix element used includes the relevant P wave Breit-Wigner curves with energy-dependent widths and arbitrary phase, and a non-resonant phase space contribution. Background under the D peak, accounted for by scaling sidebands of lower mass, is included in likelihood fit. In the $K^-\pi^+\pi^-$ case, allowance is made for the presence of two identical bosons. Figures 21-23 show the Dalitz plots of three $K\pi\pi$ decays and the relevant projections.

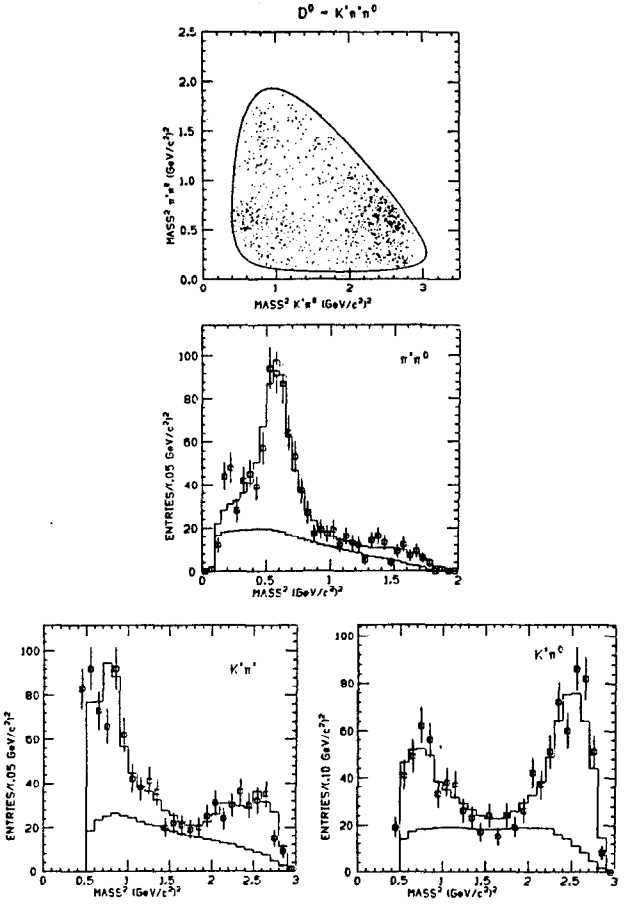

Fig. 21 Dalitz plot of the decay $D^+ \to K^-\pi^+\pi^+$, with projections.

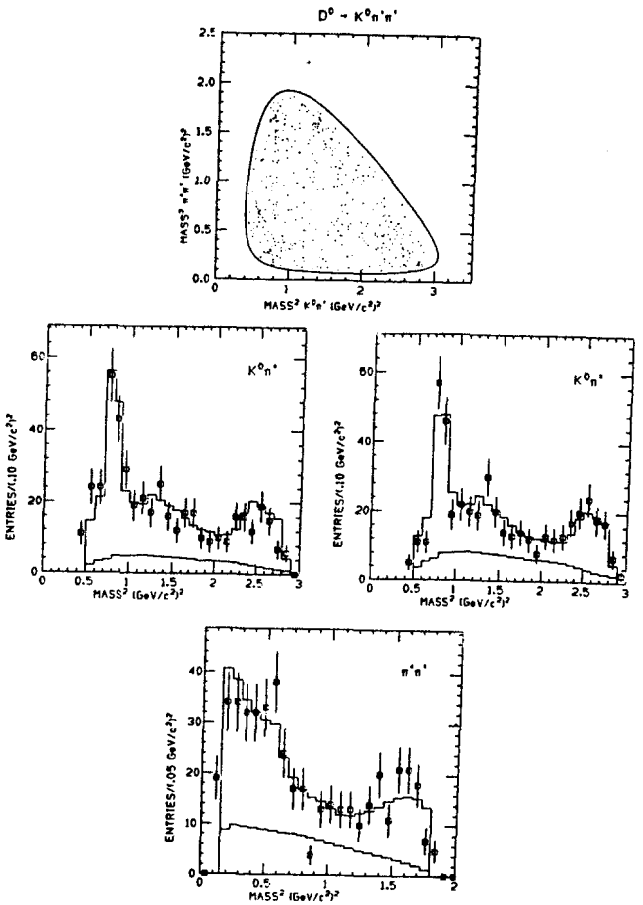

Fig. 22 Dalitz plot of the decay $D^0 \to \overline{K}^0\pi^+\pi^-$, with projections.

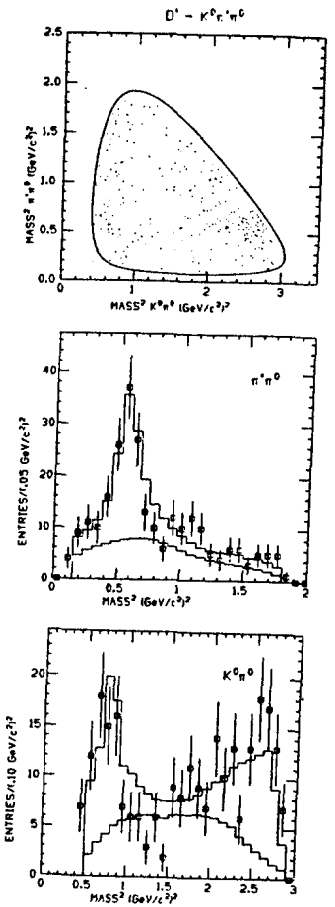

Fig. 23 Dalitz plot of the decay $D^+ \to \overline{K}^0\pi^+\pi^0$, with projections.

TABLE II

$D \to$ Pseudoscalar-Vector Branching Fractions

Channel	Source	Branching Fraction (%) Mark II[1]	TPS[29]	NA11[30]
$D \to K^*\pi$				
$D^\circ \to K^{*-}\pi^+$	$K^-\pi^\circ\pi^+$	3.6 ± 1.3	$3.4^{+3.9}_{-2.8}$	
	$\overline{K}^\circ\pi^-\pi^+$			$3.2 \pm 1.0 \pm 1.0$
$D^\circ \to \overline{K}^{*\circ}\pi^\circ$	$K^-\pi^+\pi^\circ$	$1.4^{+2.3}_{-1.4}$	$0.9^{+1.4}_{-0.9}$	
	$\overline{K}^\circ\pi^\circ\pi^\circ$			
$D^+ \to \overline{K}^{*\circ}\pi^+$	$K^-\pi^+\pi^+$	<3.7 at 90% C.L.		<1.0
	$\overline{K}^\circ\pi^\circ\pi^+$			
$D \to K\rho$				
$D^\circ \to K^-\rho^+$	$K^-\pi^+\pi^\circ$	$7.2^{+3.0}_{-3.1}$	$3.2^{+2.3}_{-1.8}$	
$D^\circ \to \overline{K}^\circ\rho^\circ$	$\overline{K}^\circ\pi^+\pi^-$	$0.1^{+0.6}_{-0.1}$		
$D^+ \to \overline{K}^\circ\rho^+$	$\overline{K}^\circ\pi^+\pi^\circ$			

The results of these fits, still preliminary, are quoted here as percentages of the appropriate $K\pi\pi$ decay mode, as studies of the normalization are as yet incomplete. Table III shows the K^* and ρ fractions extracted by this preliminary fit for three of the $K\pi\pi$ decays. The $D^\circ \to K^-\pi^+\pi^\circ$ decay shows a large $K^-\rho^+$ component, consistent with the Mark II measurement, but with substantially improved errors. This result is in poor agreement with the TPS value. A significant $K^{*-}\pi^+$ fraction and a smaller $K^{*\circ}\pi^\circ$ fraction are also observed. The $D^\circ \to \overline{K}^\circ\pi^+\pi^-$ decay, on the other hand, is dominated by $K^{*-}\pi^+$, with a smaller $\overline{K}^\circ\rho^\circ$ contribution. The $D^+ \to \overline{K}^\circ\pi^+\pi^\circ$ mode shows a very strong $\overline{K}^\circ\rho^\circ$ contribution.

TABLE III

Preliminary Mark III Results on Three $D \to PV$ Decays

Mode	PV Channel	Percent of Total
$D^\circ \to K^-\pi^+\pi^\circ$	$K^-\rho^+$	$77.1 \pm 4.9 \pm 5.0$
	$K^{*-}\pi^+$	$17.5 \pm 3.0 \pm 2.0$
	$K^{*\circ}\pi^\circ$	$5.4 \pm 2.0 \pm 2.0$
	3-body	$0.0 \pm 4.5 \pm 3.0$
$D^\circ \to \overline{K}^\circ\pi^+\pi^-$	$\overline{K}^\circ\rho^\circ$	$16.4 \pm 5.1 \pm 2.0$
	$K^{*-}\pi^+$	$66.6 \pm 8.0 \pm 5.0$
	3-body	$17.0 \pm 8.1 \pm 3.0$
$D^+ \to \overline{K}^\circ\pi^+\pi^\circ$	$\overline{K}^\circ\rho^+$	$84.0 \pm 8.5 \pm 4.0$
	$\overline{K}^{*\circ}\pi^+$	$8.6 \pm 4.7 \pm 4.0$
	3-body	$7.4 \pm 5.4 \pm 4.5$

As these results are quite preliminary, and the results of the $D^+ \to K^-\pi^+\pi^+$ analysis are not yet available, we will not at this time attempt to analyze these data in terms of the quantitative $I = \frac{1}{2}, \frac{3}{2}$ content of the $K\pi\pi$ final state. In Section 5, however, we draw some conclusions on the question of color suppression.

4.4 Absolute Branching Ratios

Measurements of the ratios of hadronic decay amplitudes are generally sufficient for an understanding of the weak decay mechanism. An understanding of charm production processes by hadrons or photons, however, requires knowledge of at least a few absolute D

decay branching ratios, in order that production cross sections be extracted from the measured $\sigma \cdot B$ for a particular channel. In the case of D studies at the Ψ'', the measurements of particular channels have in fact also been of $\sigma \cdot B$, but the clear Ψ'' enhancement in the e^+e^- hadronic cross section has made it possible to extract the resonance parameters, and thereby deduce branching ratios. This procedure is in principle straightforward, but it has in practice been limited by precision of the measurement of the Ψ'' resonance parameters.

Measurements of these parameters have been made by four groups. These are summarized in Table IV. The ratio of σ_{D^*} to σ_{D^*} is derived on the assumption that the matrix elements for D^* and $D^\pm$ pair production are equal, but that, since the Ψ'' is very close to $D\bar{D}$ threshold, the observed cross sections are influenced by the D^*–$D^\pm$ mass difference through a P_β^3 phase space dependence.

TABLE IV

Resonance Parameters and D Cross Sections of the Ψ'' (3770)

	LGW[31]	DELCO[32]	Crystal Ball[21]	Mark II[20]
Mass (MeV)	3772 ± 6	3770 ± 6		3764 ± 5
Width (MeV)	28 ± 5	24 ± 5		24 ± 5
Γ_{ee} (keV)	.37 ± .09	.18 ± .06		.276 ± .050
σ_{D^*} (nb)	11.5 ± 2.5		6.8 ± 1.2	8.0 ± 1.0 ± 1.2
σ_{D^*} (nb)	9.1 ± 2.5		6.0 ± 1.1	6.0 ± 0.7 ± 1.0
at $\sqrt{s}$(MeV) =	3774		3771	3771

The Mark III did not attempt a measurement of the Ψ'' resonance parameters, preferring to gather the largest D sample possible in the running time available at $\sqrt{s} = 3768$ MeV. Thus extraction of D branching ratios from the measured $\sigma \cdot B$ values (Table I) was done by using $\sigma_{D^*} = 7.5 \pm 1.1 \pm 1.2$ nb and $\sigma_{D^*} = 6.0 \pm 0.9 \pm 1.0$ nb, the average of the Crystal Ball and Mark II measurements. Since the values of $\sigma \cdot B$ obtained are generally in good agreement with those previously measured, albeit with improved precision, the derived branching ratios are also in agreement.

The large discrepancies in the measured σ_{D^*} and σ_{D^*} values, however, prompted us to turn to a new technique, which allows an absolute measurement of the D hadronic branching ratios. The data sample is sufficiently large and the D reconstruction efficiency of the Mark III is sufficiently high, that it is possible to measure branching ratios using completely reconstructed $D\bar{D}$ events. These are termed "doubly tagged" as opposed to events in which a single D hadronic decay is reconstructed, which are termed "singly tagged." By taking the ratio of doubly tagged to singly tagged events, it is possible to extract the absolute branching fraction, independent of σ_D. Final results using this technique will employ all possible combinations of different decay modes in which the signal to background ratio is sufficiently high. The preliminary results presented here, however, require that the D and $\bar{D}$ decay into the same final state. The doubly tagged channels used are

$$\Psi'' \longrightarrow D^*\bar{D}^* \begin{cases} \longrightarrow K^+\pi^- \\ \longrightarrow K^-\pi^+ \end{cases},$$

and

$$\Psi'' \longrightarrow D^+D^- \begin{cases} \longrightarrow K^+\pi^-\pi^- \\ \longrightarrow K^-\pi^+\pi^+ \end{cases}.$$

The number of single tagged events into a particular channel is

$$N_1 = N(D_{\text{produced}}) \times B(D \rightarrow \text{tag}) \times \varepsilon(\text{tag}),$$

while the number of doubly tagged events into that channel is

$$N_2 = N_1 \times B(\bar{D} \to \text{tag}) \times \varepsilon(\text{recoil tag}) \ .$$

Thus the absolute branching fraction is given by

$$B(\bar{D} \to \text{tag}) = N_2/(N_1 \times \varepsilon(\text{recoil tag})) \ .$$

The sample used in this analysis differs slightly from that used for the conventional analysis. Doubly tagged events are isolated by choosing those single tagged events into a given channel which have the correct topology, a recoil momentum within 50 MeV of the expected value, good K,π mass assignments and an invariant recoil mass equal to that of the D within the experimental resolution. After these selection criteria are applied, the beam-constrained mass of the recoil is plotted against that of the tag. This is shown in Figures 24 and 25 for the D^* and D^+ channels investigated here. A clear doubly tagged signal is seen in both cases, with a small uniform background from continuum production and random track combinations.

The absolute branching fractions for these two modes are then extracted using the procedure described above. The results are summarized in Table V.

TABLE V

Absolute Branching Fractions for Two D Decay Modes

Channel	Singly Tagged Events	Doubly Tagged Events	Background Events	Recoil Tag Efficiency	B(%)
$D^* \to K^-\pi^+$	978 ± 33	29 ± 6	1.7	.61	4.9 ± 0.9 ± 0.5
$D^+ \to K^-\pi^+\pi^+$	1109 ± 37	46 ± 7	2.2	.45	9.1 ± 1.5 ± 0.9

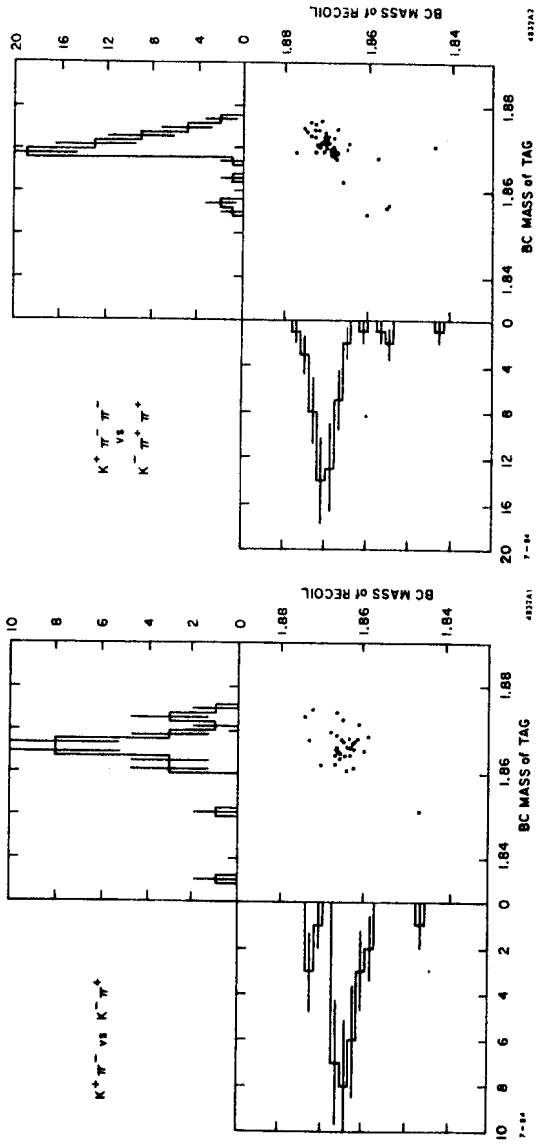

Fig. 24 Beam constrained mass of $K^-\pi^+$ vs that of $K^+\pi^-$, and projections, showing evidence for completely reconstructed events of the type $\Psi'' \to D^*\bar{D}^*$; $D^* \to K^-\pi^+$, $\bar{D}^* \to K^+\pi^-$.

Fig. 25 Beam constrained mass of $K^-\pi^+\pi^+$ vs that of $K^+\pi^-\pi^-$, and projections, showing evidence for completely reconstructed events of the type $\Psi'' \to D^+D^-; D^+ \to K^-\pi^+\pi^+$, $D^- \to K^+\pi^-\pi^-$.

The branching fractions so obtained are completely independent of σ_D, having errors given by statistics and the uncertainty in the recoil tag efficiency, which is estimated by Monte Carlo. These branching fractions are larger than those extracted by the conventional technique, shown in Table I, which used an average of Mark II and Crystal Ball values for σ_D. Given the difficulty in measuring the D production cross section at the Ψ'', the absolute determinations are likely to provide the more reliable values. It is interesting to combine the absolute branching fractions of Table V with the $\sigma \cdot B$ determinations of Table I to independently derive the D production cross sections. The values so obtained are

$$\sigma_{D^0} = 5.7 \pm 1.1 \pm 0.9 ,$$

$$\sigma_{D^+} = 4.6 \pm 0.8 \pm 0.7 ,$$

at $\sqrt{s} = 3768$ MeV. These cross sections are substantially lower than those from any of the direct measurements, although the errors on the two techniques are, at this point, comparable.

Table VI is a comparison of the D branching fractions for the $K^-\pi^+$ and $K^-\pi^+\pi^+$ modes derived from the older $\sigma \cdot B$ measurements and the new absolute method described above.

The following points should be noted. All three determinations of $\sigma \cdot B$ for these modes show excellent agreement, the difference between Lead Glass Wall and Mark II values of B arising essentially from differences in σ_D. The Mark III branching fractions determined by the $\sigma \cdot B$ method are larger than previous measurements for two reasons: the actual $\sigma \cdot B$ values are very slightly larger, and different values for σ_D, derived from averaged Mark II and Crystal Ball determinations, were used to extract the branching fraction. Note also that the two determinations by the Mark III are consistent within experimental error. Despite the relatively good agreement among individual measurements, if viewed in historical progression, the net result of the new Mark III measurements of absolute branching fractions is dramatic: charm production cross sections in both hadron and photon beams, if extracted from $\sigma \cdot B$ measurements using the Particle Data Group averages of LGW and Mark II data, **must be reduced by more than a factor of two**.

TABLE VI

Comparison of Two Methods of Measurement of D Hadronic Branching Fractions

Mode		$\sigma \cdot B$ Method				Double Tag Method
		LGW	Mark II	PDG Value	Mark III	Mark III
$D^0 \to K^-\pi^+$	B(%)	2.2 ± 0.6	3.0 ± 0.6	2.4 ± 0.4	$3.7^{\pm 0.9}_{\pm 0.7}$	4.9 ± 0.9 ± 0.5
	$\sigma \cdot B$(nb)	0.25 ± 0.05	0.24 ± 0.02		$0.28^{\pm 0.01}_{\pm 0.3}$	
$D^+ \to K^-\pi^+\pi^+$	B(%)	3.9 ± 1.0	6.3 ± 1.5	4.6 ± 1.1	$7.0^{\pm 1.1}_{\pm 1.3}$	9.1 ± 1.5 ± 0.9
	$\sigma \cdot B$(nb)	0.36 ± 0.06	0.38 ± 0.05		$0.42^{\pm 0.02}_{\pm 0.04}$	

4.5 Semileptonic Decays

Semileptonic decays of hadrons have historically provided important tests of our understanding of weak decay mechanisms. Matrix elements for these decays, being the product of a lepton and a hadron current, are simpler to calculate than those for hadronic decays.[32] In the case of K decays, the semileptonic modes have provided tests of the $\Delta S = \Delta Q$ rule, CP invariance, μ–e universality and chiral symmetry. Charmed particle semileptonic decays provide a similarly rich array of possibilities, although experiments to data have been limited to studies of inclusive lepton spectra and semileptonic branching

ratios. In the near future, Mark III studies of D_{e3} and $D_{\mu 3}$ Dalitz plots will provide information on branching ratios to specific hadron final states, such as $D \to Klv$ and $D \to K^*lv$, as well as information on the q^2 dependence of some of the form factors governing these exclusive decays. The results presented here, however, will be limited to improved measurements of individual branching fractions and inclusive electron spectra for the D^* and D^+ semileptonic decays.

Semileptonic branching ratios yield direct insight into the charm weak decay process. Naively, one would expect an ~20% semileptonic branching ratio just from counting lepton species and quark colors. As an enhancement of the non-leptonic sector is an established feature of K decays, such an enhancement is also expected in D decays, and the renormalization of the c_+ and c_- operator coefficients indeed, as we have seen, predicts this. With the corrected leading log values, this enhancement, however, is relatively small, so that $B(c \to (e \text{ or } \mu) + X)$ is predicted to be 13-16%. In this picture, the semileptonic branching ratios of the D^*, D^+ and F^+ are, of course, identical. Should the lifetimes of charmed particles differ, however, then their semileptonic branching fractions will differ in the same proportion. To the extent that the semileptonic decay is a spectator process, we expect equal semileptonic decay widths and thus the ratio of semileptonic branching fractions is just the ratio of the lifetimes.

It is important to note that as long as measurements are limited to inclusive electron tagging, the Cabibbo-suppressed D^+ semileptonic decay process (Fig. 3b) can contribute to $\Gamma(D^+ \to e^+X)$, and the equality of the ratios described above is valid only to the extent that this additional decay process can be ignored. The new measurements of Cabibbo-suppressed D^+ hadronic decays described above make it certain that the Cabibbo-suppressed D^+ semileptonic width is much less than 10% of the allowed semileptonic width, and thus, at the level of precision of current experiments, can be ignored. Figure 26 shows the dominant Cabibbo-allowed and -suppressed exclusive decays which contribute to the inclusive

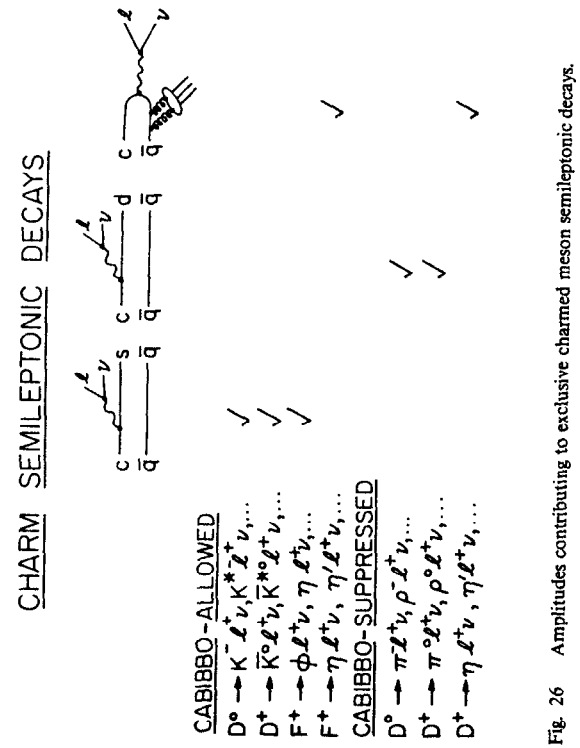

Fig. 26 Amplitudes contributing to exclusive charmed meson semileptonic decays.

semileptonic decay width.

The technique employed for semileptonic decay studies in the Mark III is similar to that used to measure absolute hadronic branching fractions. That is, a hadronic D decay is first reconstructed, thus determining unambiguously the charm of the so-called tagged state, and then, taking advantage of the dominance of $D\bar{D}$ production at the Ψ'', the recoil spectrum is studied to isolate leptons of the correct sign which originate from a semileptonic decay of the recoil D meson. This technique was first employed by the Mark II, which showed that the D° and D^+ semileptonic branching fractions were not, as expected, equal. The Mark III analysis offers increased statistics and improved electron identification, leading to a substantially improved measurement.

The tag sample, reconstructed using a total of 8.6 pb^{-1} collected at the Ψ'', consists of three D° channels ($K^-\pi^+$, $K^-\pi^+\pi^\circ$ and $K^-\pi^+\pi^+\pi^-$) and two D^+ channels ($\bar{K}^\circ\pi^+$ and $K^-\pi^+\pi^+$), reconstructed using the beam-constraint method described earlier. In each of these mass plots a signal region centered on the D mass and a control region used to correct for background events other than the signal, are defined. The number of background events under each signal is determined by a fit to the mass plot. The D° signal contains 4541 events, of which 1106 ± 34 are background, while the D^+ signal contains 2062 events of which 333 ± 20 are background.

Tracks recoiling against these reconstructed D's are then classified as electrons or pions by a binary tree algorithm. Candidate recoil tracks must have $p > 150$ MeV/c, originate near the primary vertex and lie in a fiducial region $|\cos\theta| < 0.77$, which permits charged K's and p's to be rejected by time-of-flight measurement. Further cuts remove Dalitz decays and photon conversions. Electron/pion separation is then accomplished in various momentum intervals by a series of cuts on time-of-flight and shower development profiles which have been optimized using pure e and π samples from the J/ψ. Actual misidentification rates, which average about 2.5%, were measured using a pion sample from K_s° decay and an electron sample from radiative Bhabha events at the Ψ''.

The charm of the reconstructed D unambiguously determines the charge of the recoil electron. It is thus possible to use this fact to correct for backgrounds. Correction for charge symmetric sources such as remaining Dalitz decays and photon conversions are made by subtracting the number of "wrong-sign" candidates from the number of "right-sign" candidates, i.e., those with the expected charge. The background contributed by pion misidentification rates to unfold the actual number of electrons from the observed number of electron and pion candidates of each sign. This background amounts to 20% for the D^+ and 14% for the D°. Further corrections must then be made for background events under the hadronic D signals, TOF misidentification of K and π in the $D^\circ \to K^-\pi^+$ channel and K_{e3} decays. The efficiency of this process is 70% for electrons from both D^+ and D°. Table VII summarizes the electron identification procedure and the corrections discussed above. The electron spectra so determined are shown, after background subtraction, in Fig. 27, along with the spectra expected from $D \to Kev$ and K^*ev decays.[33]

TABLE VII

Recoil Electron Identification

Source	Signal Events (Tags)	Right Sign Recoil Electrons	Wrong Sign Recoil Electrons	Control Region Electrons	Net Signal Electrons	Signal Electrons Corrected for Efficiency
D°	3435 ± 39	193 ± 13.9	57.0 ± 7.5	5.2 ± 4.5	136.6 ± 20.4	251.7 ± 37.9
D^+	1729 ± 20	177 ± 13.3	14.0 ± 3.7	2.5 ± 2.9	158.2 ± 17.6	294.0 ± 32.6

The number of correct sign recoil electrons observed leads to the branching fractions:

$$B(D^+ \to e^+ + X) = (17.0 \pm 1.9 \pm 0.7)\%$$

and

$$B(D^\circ \to e^+ + X) = (7.5 \pm 1.1 \pm 0.4)\%\,,$$

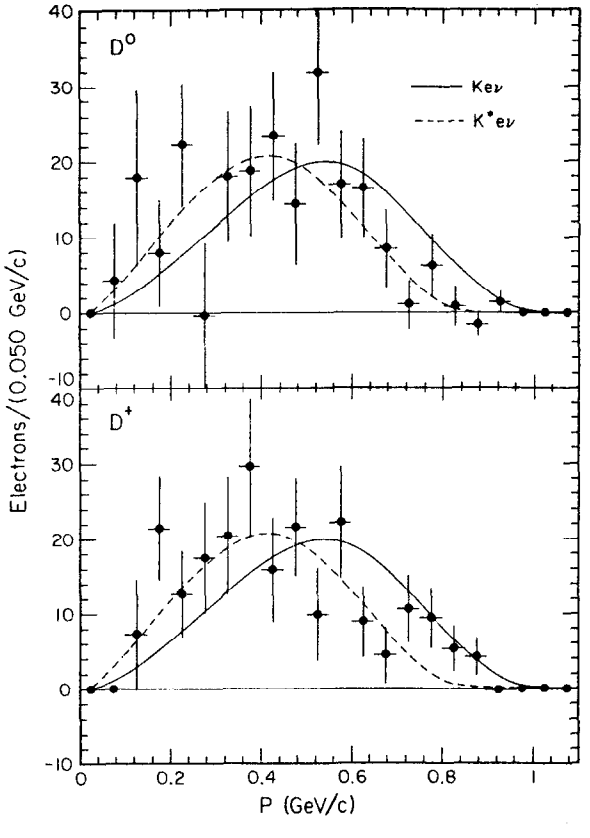

Fig. 27 Electron recoil spectra in D^* and D^+ decays after efficiency correction, together with spectra expected for $D \to Ke\nu$ and $D \to K^*e\nu$.

and thus to the ratio

$$\frac{B(D^+ \to e^+ + X)}{B(D^* \to e^+ + X)} = 2.3^{+0.5+0.1}_{-0.4-0.1} .$$

Note that several sources of systematic error cancel in the ratio of branching fractions.

The new Mark III measurements thus yield an average D semileptonic branching ratio at the Ψ'' of (11.7 ± 1.0 ± 0.5)%. This is consistent with the Mark II value[1] of (10.0 ± 3.2)%, derived using the same absolute normalization technique, but substantially higher than the DELCO[2] ((8.0 ± 1.5)%) and the LGW[34] ((7.2 ± 2.8)%) determinations, which relied on normalization of the electron signal to the measured Ψ'' cross section. As shown above, absolute measurements as made by the Mark III for hadronic branching fractions also yield larger values. These changes are significant, not only for an understanding of the weak decay process, but also for the effect they have on extraction of the charmed sea component measured in neutrino interactions.

The likelihood function for the ratio of semileptonic branching fractions is shown in Fig. 28. Interpreted as the ratio of D^+ to D^* lifetimes with the assumptions discussed above, the new Mark III measurement thus excludes equal lifetimes at the 4.3 standard deviation level. The ratio of 2.3 agrees well with the world average of less precise separate measurements of the D^+ and D^* lifetimes.

5. DISCUSSION

The new Mark III results on inclusive and exclusive D decay processes allow us, at least in broad outline, to describe the weak decay for charmed particles in a consistent way. Many of these results are preliminary, so an exhaustive analysis will not be attempted here. Let us focus first on inclusive phenomena.

It is now quite clear that the D^+ lifetime is longer than the D^* lifetime by more than a factor of two. The D^+ semileptonic branching ratio is close to that expected with

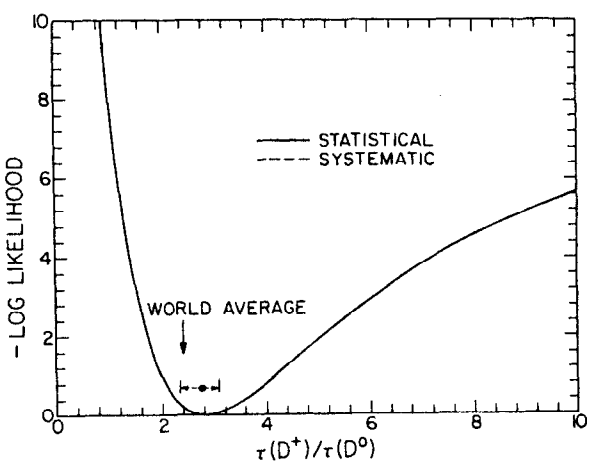

Fig. 28 Likelihood function for the ratio of semileptonic branching fractions.

renormalized operator coefficients, radiative corrections and quark mass corrections. Indeed, were we to use only leading log values of c_+ and c_- and neglect the Pauli interference, we would conclude that the D^+ width was essentially the expected value. Figure 29 compares the Mark III measured value of $B(D^+ \to e^+X)$ with that expected for differing values of c_-/c_+, with the interference term parametrized by a coefficient α as defined in Section 3. We see that the data is well represented with either LL values of c_- and c_+ and $\alpha = 0$, or with $c_-/c_+ \sim 3.5$ and $\alpha \sim 0.5$. The relation between α and f_D is, of course, model dependent, but an f_D of 200-300 MeV, only somewhat larger than most expectations, would typically generate $\alpha \sim 0.5$. The value of c_-/c_+ is quite plausible when next-to-leading log terms are included. (Soft gluon effects not calculable by QCD perturbative techniques also tend to increase c_-/c_+.) Thus D^+ decay appears to be relatively "normal", i.e., it is well described by a spectator model, providing expected corrections to the naive model are accounted for.

The D^* semileptonic branching ratio, on the other hand, is much smaller than can be accounted for in the spectator model. It is more than a factor of two smaller than the naive spectator prediction with leading log renormalization of c_- and c_+. It is nonetheless possible to arrive at a consistent picture for the D^* width. With the inclusion of NLL modifications to c_-/c_+, it is possible to bring down $B(D^* \to e^+X)$ to the region of 11-12%. If we also include the contribution of the exchange diagram, parametrized in Fig. 30 in a model in which lifting of helicity suppression is ascribed to the intrinsic gluon component of the meson wave function,[16] it is possible to increase the D^* width sufficiently to account for the measured D^* semileptonic branching ratio with values of f_D again in the range of 200-300 MeV. Thus, the ratio of D^+ to D^* lifetimes can be understood in a consistent way. We require that the QCD hard gluon corrections to c_- and c_+ be calculated beyond the leading log approximation, that Pauli interference in D^+ decay be included and that the gluon content of the D meson wavefunction be sufficiently large to negate the helicity suppression of the naive spectator model, allowing W exchange amplitudes to contribute to D^* decay.

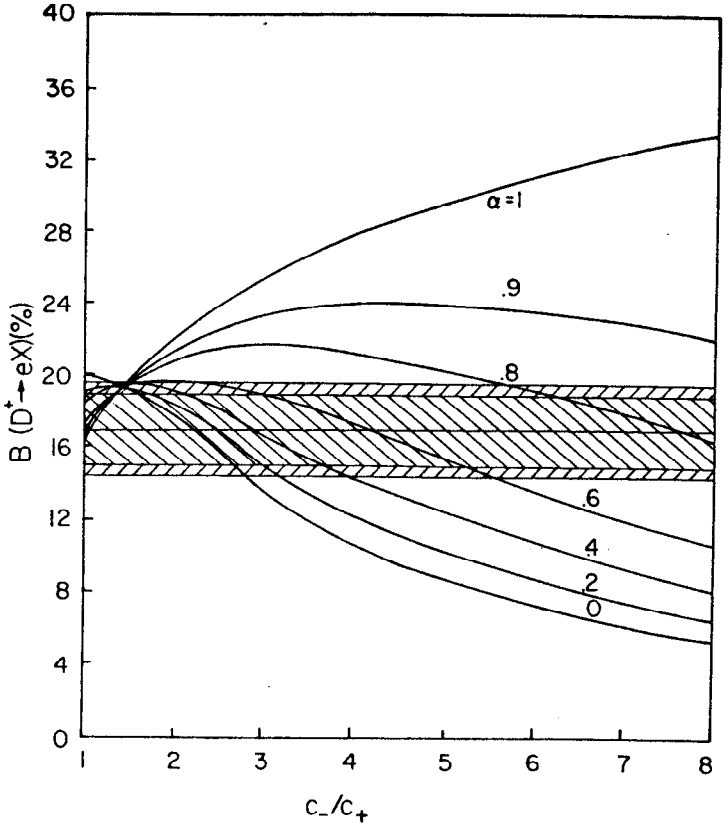

Fig. 29 The D^+ semileptonic branching fraction as a function of c_-/c_+ for different values of the parameter α which governs the amount of Pauli interference. The Mark III experimental result with statistical and systematic uncertainties is superimposed.

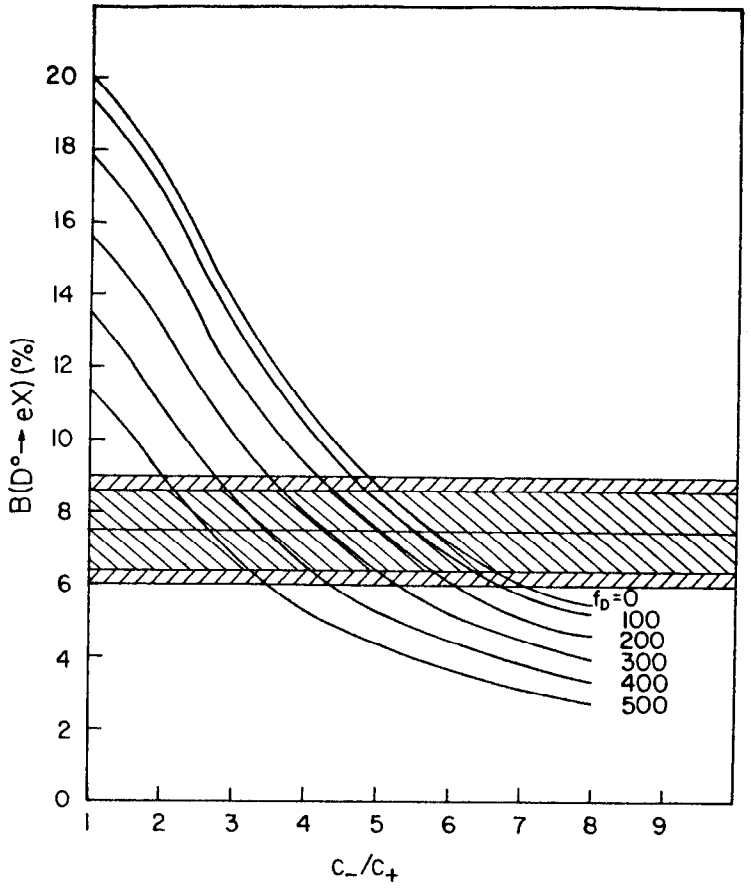

Fig. 30 The D^* semileptonic branching fraction as a function of c_-/c_+ for different values of f_D in a model which parametrizes the lifting of helicity suppression of the exchange amplitude in terms of the singlet component of the gluon wave function of the D^*. The Mark III experimental result with statistical and systematic uncertainties is superimposed.

As this picture is only semi-quantitative, no attempt has been made to extract the overall best values of f_D and c_-/c_+ by fitting simultaneously to the measured D^+ and D° semileptonic branching ratios. It is possible, however, to ensure ourselves of the consistency of these ideas by looking at exclusive D decays.

Three ratios which are sensitive to the existence of color suppression and the isospin content of the final state may be extracted from the new Mark III hadronic branching ratios. These are

$$R(K\pi) = \frac{\Gamma(D^\circ \to \overline{K}^\circ\pi^\circ)}{\Gamma(D^\circ \to K^-\pi^+)} = 0.35 \pm 0.07 \pm 0.07,$$

$$R(K^*\pi) = \frac{\Gamma(D^\circ \to \overline{K}^{*\circ}\pi^\circ)}{\Gamma(D^\circ \to K^{*-}\pi^+)} = 0.15 \pm 0.09 \text{ , and}$$

$$R(K\rho) = \frac{\Gamma(D^\circ \to \overline{K}^\circ\rho^\circ)}{\Gamma(D^\circ \to K^-\rho^+)} = 0.16 \pm 0.07 \text{ .}$$

In the limit of a pure $I = \frac{1}{2}$ final state, these ratios would be $\frac{1}{2}$. Were color suppression operative, all three ratios would be very small. As there is no evidence for W exchange amplitudes in exclusive channels (cf. $D^\circ \to \overline{K}^\circ\varphi$) we will henceforth assume that the amplitude g of Sec. 3.2 is zero, leaving only the contribution of spectator diagrams, characterized by c_- and c_+. These experimental ratios are then very sensitive to the value of c_-/c_+. Figure 31 shows the three ratios $R(K\pi)$, $R(K^*\pi)$ and $R(K\rho)$ as a function of c_-/c_+. The naive spectator model ($c_-/c_+ = 1$) predicts 1/18. The LL prediction is actually less. As c_-/c_+ increases beyond 2, R increases. While there is no point at which the three ratios are compatible with a single value of c_-/c_+, it is clear that values in the range needed to explain the semileptonic data are consistent with the large R values observed. Since the pseudoscalar-vector decays are $L = 1$, the enhancement here would be expected to be less than that for $\overline{K}^\circ\pi^\circ$, in accord with observation. Should exchange diagrams contribute, they would also be expected to be larger for $L = 1$ than $L = 0$.

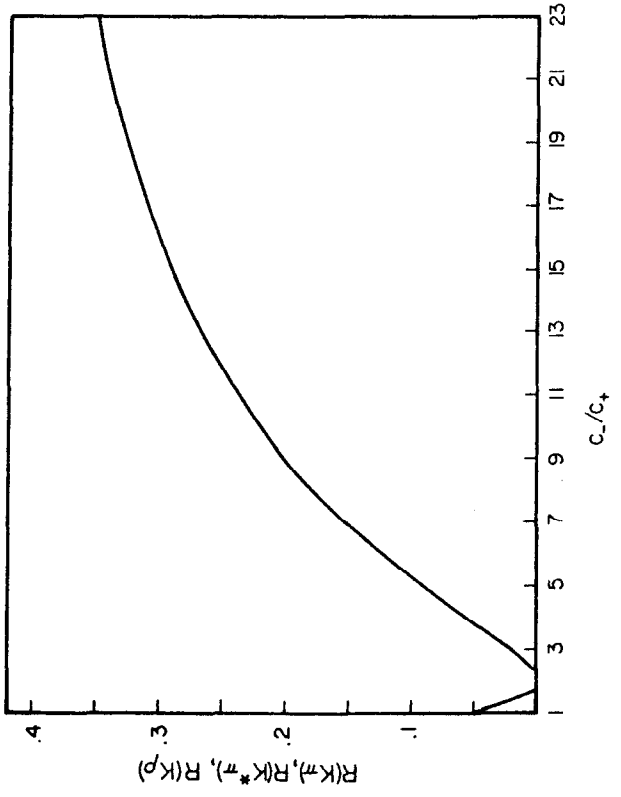

Fig. 31 The ratio $R(K\pi)$, $R(K^*\pi)$, $R(K\rho)$ as a function of c_-/c_+.

Recall also that the Cabibbo-suppressed decay $D^+ \to \varphi\pi^+$, which is also naively color suppressed, occurs at a normal suppressed rate. Again, color suppression is not operating strongly.

A final comparison will serve to further bolster the argument that the physical value of c_-/c_+ is not properly given by the leading log calculation. Consider the ratio of allowed decays

$$\frac{\Gamma(D^* \to K^-\pi^+)}{\Gamma(D^+ \to \overline{K}^{*}\pi^+)} = \left[\frac{2c_+ + c_-}{4c_+}\right]^2 ,$$

and the ratio

$$\frac{\Gamma(D^+ \to \overline{K}^{*}K^+)}{\Gamma(D^+ \to \overline{K}^{*}\pi^+)} = \left[\frac{2c_+ + c_-}{4c_+}\right]^2 \left|\frac{V_{us}^*}{V_{ud}^*}\right|^2 .$$

Both are dependent on SU(3) breaking and the interference of color-mixed and -unmixed amplitudes (Fig. 5). Both ratios are far larger than expected in the LL picture. Figure 32 compares these experimental ratios with predictions as a function of c_-/c_+. In both cases, large values of c_-/c_+ are required to explain the observations.

We thus are led to a consistent picture of the weak decay mechanism for charmed mesons. When all expected effects are properly incorporated, the nonequality of D^+ and D^* lifetimes and the ratios of a large number of exclusive branching fractions are most simply explained by a picture in which the ratio of the operator coefficients c_- and c_+ is larger than that calculated in leading log QCD, at least part of the increase being due to the next-to-leading log terms, which increase c_-/c_+ to ~3.5. It is further possible that non-perturbative soft gluon effects also play a role in increasing c_-/c_+ beyond this value. While precise calculations do not exist, estimates show that these effects indeed increase c_-/c_+.

As the results presented here are largely preliminary, no attempt has been made to extract a best value of c_-/c_+ through a global fit to the inclusive and exclusive data. Several

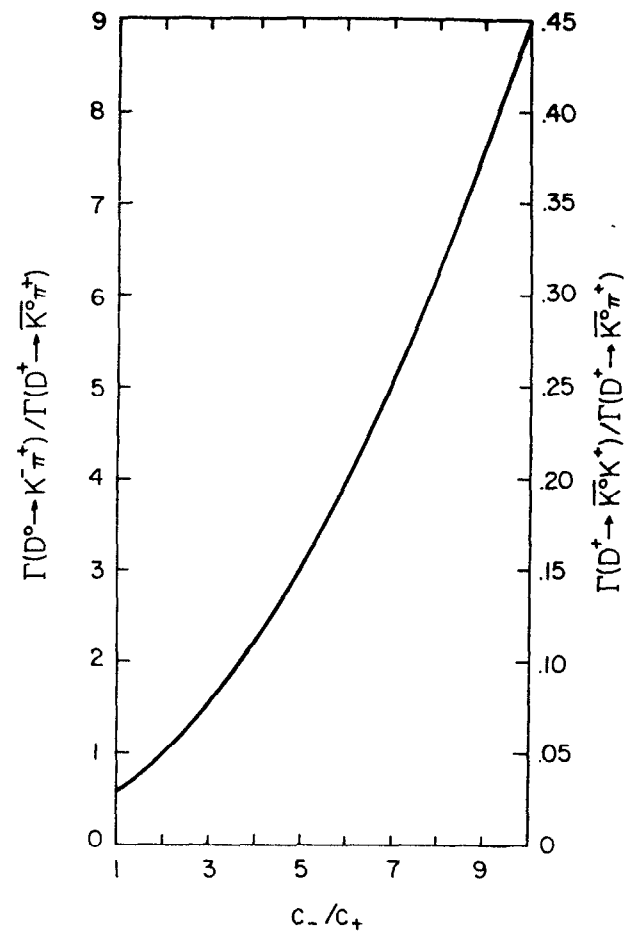

Fig. 32 The ratio $\Gamma(D^* \to K^-\pi^+)/\Gamma(D^+ \to \overline{K}^{*}\pi^+)$ (left scale), and $\Gamma(D^+ \to \overline{K}^{*}K^+)/\Gamma(D^+ \to \overline{K}^{*}\pi^+)$ (right scale) as a function of c_-/c_+.

discussions of these preliminary Mark III results have, however, already appeared in the literature.[35]

6. ACKNOWLEDGEMENTS

The data discussed herein is the work of the Mark III Collaboration at SPEAR. I would like to acknowledge helpful conversations with, among others, I. Bigi, H. Fritzsch, F. Gilman, A. Kamal, M. Peskin, M. Scadron, R. Schindler, B. Stech, R. Rückl and M. Wise.

REFERENCES

*The members of the Mark II Collaboration are:

R. M. Baltrusaitis, J. J. Becker, G. T. Blaylock, J. S. Brown, K. O. Bunnell, T. H. Burnett, R. E. Cassell, D. Coffman, V. Cook, D. H. Coward, S. Dado, C. Del Papa, D. E. Dorfan, G. P. Dubois, A. L. Duncan, K. F. Einsweiler, B. I. Eisenstein, R. Fabrizio, G. Gladding, F. Grancagnolo, R. P. Hamilton, J. Hauser, C. A. Heusch, D. G. Hitlin, L. Koepke, W. S. Lockman, P. M. Mockett, L. Moss, R. F. Mozley, A. Nappi, A. Odian, R. Partridge, J. Perrier, S. A. Plaetzer, J. D. Richman, J. R. Roehrig, J. J. Russell, H. F. W. Sadrozinski, M. Scarlatella, T. L. Schalk, R. H. Schindler, A. Seiden, J. C. Sleeman, A. L. Spadafora, J. J. Thaler, W. Toki, B. Tripsas, F. Villa, A. Wattenberg, A. J. Weinstein, N. Wermes, H. J. Willutzki, D. E. Wisinski, W. J. Wisniewski

1) R. H. Schindler *et al., Phys. Rev.* **D24**, 78 (1981).

2) W. Bacino *et al., Phys. Rev. Lett.* **45**, 329 (1980).

3) G. S. Abrams *et al., Phys. Rev. Lett.* **43**, 481 (1979).

4) For a detailed discussion, see, for example, R. Klanner, *Proceedings of the XXII International Conference on High Energy Physics* (Leipzig, 1984).

5) D. Bernstein *et al., Nucl. Instr. Meth.* **226**, 301 (1984).

6) A. Pais and S. B. Treiman, *Phys. Rev.* **D15**, 2529 (1977).

7) J. Ellis, M. K. Gaillard and D. V. Nanopoulos, *Nucl. Phys.* **B100**, 313 (1975).

8) R. Kingsley, S. Treiman, F. Wilczek and A. Zee, *Phys. Rev.* **D11**, 1919 (1975);
J. F. Donoghue and B. R. Holstein, *Phys. Rev.* **D12**, 1454 (1975);
M. B. Einhorn and C. Quigg, *Phys. Rev.* **D12**, 2015 (1975);
G. Altarelli, N. Cabibbo and L. Maiani, *Nucl. Phys.* **B88**, 285 (1975).

9) M. K. Gaillard and B. W. Lee, *Phys. Rev. Lett.* **33**, 108 (1974);
G. Altarelli and L. Maiani, *Phys. Lett.* **52B**, 351 (1974).

10) G. Altarelli, G. Curci, G. Martinelli and R. Petrarca, *Phys. Lett.* **99B**, 141 (1981) and *Nucl. Phys.* **B187**, 461 (1981).

11) N. Cabibbo and L. Maiani, *Phys. Lett.* **79B**, 109 (1978);
M. Suzuki, *Nucl. Phys.* **B145**, 420 (1978);
N. Cabibbo, G. Corbo and L. Maiani, *Nucl. Phys.* **B155**, 93 (1979);
A. Ali and E. Pietarinen, *Nucl. Phys.* **B154**, 591 (1979);
G. Corbo, *Phys. Lett.* **116B**, 298 (1982) and *Nucl. Phys.* **B122**, 99 (1982);
Q. Ho-Kim and X.-Y. Pham, CERN preprint Th. 3417 (1982).

12) N. Deshpande, M. Gronau and D. Sutherland, *Phys. Lett.* **90B**, 431 (1980);
M. Gronau and D. Sutherland, *Nucl. Phys.* **B183**, 367 (1981);
Y. Igarashi, M. Kuroda and S. Kitakado, *Phys. Lett.* **97B**, 269 (1980);
R. Rückl, MPI-PAE/PTh 23/80.

13) B. Guberina, S. Nussinov, R. D. Peccei and R. Rückl, *Phys. Lett.* **89B**, 111 (1979);
R. D. Peccei and R. Rückl, in *Proceedings of the Ahrenshoop Symposium on Special Topics in Gauge Field Theories*, Akad. d. Wiss. der DDR (Berlin, 1981);
V. A. Khoze and M. A. Shifman, *Uspekki. Fiz. Nauk.* **10**, 2 (1983) and DESY 83-105;
T. Kobayashi and N. Yamazaki, *Proc. Theor. Phys.* **65**, 775 (1981);
H. Sawayanagi, K. Fujii, T. Okazaki and S. Okubo, *Phys. Rev.* **D27**, 2107 (1983);
N. Bilić, B. Guberina and J. Trampetić, MPI-PAE/PTh 28/84;
G. Altarelli and L. Maiani, *Phys. Lett.* **118B**, 414 (1982);
M. A. Shifman and M. B. Voloshin, ITEF 84-62.

14) W. Bernreuther, O. Nachtmann and B. Stech, *Z. Physik* **C4**, 455 (1980);
I. I. Bigi, *Z. Physik* **C5**, 313 (1980);
V. Barger *et al., Phys. Rev.* **D22**, 693 (1980);
S. P. Rosen, *Phys. Rev. Lett.* **44**, 4 (1980).

15) M. Bander, D. Silverman and A. Soni, *Phys. Rev. Lett.* **44**, 7 (1980);
Erratum: *Phys. Rev. Lett.* **44**, 962 (1980).

16) H. Fritzsch and P. Minkowski, *Phys. Lett.* **90B**, 455 (1980).

17) K. Shizuya, *Phys. Lett.* **100B**, 79 (1981) and *Phys. Lett.* **105B**, 406 (1981).

18) I. I. Bigi and M. Fukugita, *Phys. Lett.* **91B**, 121 (1980);
M. Bace and X.-Y. Pham, *Phys. Lett.* **98B**, 211 (1981).

19) H. J. Lipkin, ANL-HEP-CP-80-64.

20) R. H. Schindler *et al., Phys. Rev.* **D21**, 2716 (1980).

21) H. Sadrozinski, *Proceedings of the XX International Conference on High Energy Physics*, (Madison, 1980).

22) I. Peruzzi *et al., Phys. Rev. Lett.* **39**, 1301 (1977);
D. L. Sharre, *Phys. Rev. Lett.* **40**, 74 (1978).

23) R. Rückl, Habilitationsschrift, University of Munich (1983).

24) I. I. Bigi, PITHA 82/07 (1982).

25) V. Barger and S. Pakvasa, *Phys. Rev. Lett.* **43**, 812 (1979);
L.-L. Chau and F. Wilczek, *Phys. Rev. Lett.* **43**, 816 (1979);
M. Suzuki, *Phys. Rev. Lett.* **43**, 818 (1979) and *Phys. Lett.* **85B**, 91 (1980);
G. Kane, SLAC-PUB-2326 (1979);
L. F. Abbott, P. Sikivie and M. Wise, *Phys. Rev.* **D21**, 1393 (1980);
D. G. Sutherland, *Phys. Lett.* **90B**, 173 (1980);
J. F. Donoghue and B. R. Holstein, *Phys. Rev.* **D21**, 1334 (1980);
H. J. Lipkin, *Phys. Rev. Lett.* **44**, 710 (1980);
L. Wolfenstein, Carnegie-Mellon Preprint C00-3066-134

26) For a review, see G. Wolf, *Proceedings of the XXII International Conference on High Energy Physics* (Leipzig, 1984).

27) M. Fukugita, T. Hagiwara and A. Sanda, RHEL-79-052 (1979);
J. Finjord, *Nucl. Phys.* **B181**, 74 (1981);
M. Glück, *Phys. Lett.* **88B**, 145 (1979);
L. F. Abbott, P. Sikivie and M. Wise, *Phys. Rev.* **D21**, 768 (1980).

28) L.-L. Chau, *Phys. Reports* **95**, 1 (1983).

29) D. J. Summers *et al.*, *Phys. Rev. Lett.* **52**, 410 (1984).

30) R. Bailey *et al.*, *Phys. Lett.* **132B**, 237 (1983).

31) P. A. Rapidis *et al.*, *Phys. Rev. Lett.* **39**, 526 (1977).

32) W. Bacino *et al.*, *Phys. Rev. Lett.* **40**, 671 (1978).

33) A. Ali, *Phys. Lett.* **65B**, 275 (1976).

34) J. Feller *et al.*, *Phys. Rev. Lett.* **40**, 374 (1978).

35) R. Rückl, *Proceedings of the XXII International Conference on High Energy Physics*, (Leipzig, 1984);
M. Bauer and B. Stech, Heidelberg Preprint HD-THEP-84-22;
A. Kamal, SLAC-PUB-3443.